Engineering chitinolytic activity into a cellulose-active lytic polysaccharide monooxygenase provides insights into substrate specificity

Marianne Slang Jensen[1], Geir Klinkenberg[2], Bastien Bissaro[1], Piotr Chylenski[1], Gustav Vaaje-Kolstad[1], Hans Fredrik Kvitvang[2], Guro Kruge Nærdal[2], Håvard Sletta[2], Zarah Forsberg[1,*], Vincent G.H. Eijsink[1,*]

[1]Faculty of Chemistry, Biotechnology and Food Science, NMBU - Norwegian University of Life Sciences, Ås, Norway
[2]SINTEF Industry, Department of Biotechnology and Nanomedicine, Trondheim, Norway

Running title: *Engineering LPMO substrate specificity*

[*]For correspondence; E-mail: zarah.forsberg@nmbu.no & vincent.eijsink@nmbu.no

ABSTRACT

Lytic polysaccharide monooxygenases (LPMOs) catalyze oxidative cleavage of recalcitrant polysaccharides such as cellulose and chitin and play an important role in the enzymatic degradation of biomass. While it is clear that these monocopper enzymes have extended substrate-binding surfaces for interacting with their fibrous substrates, the structural determinants of LPMO substrate specificity remain largely unknown. To gain additional insight into substrate specificity in LPMOs, here we generated a mutant library of a cellulose-active family AA10 LPMO from *Streptomyces coelicolor* A3(2) (*Sc*LPMO10C, also known as CelS2) having multiple substitutions at five positions on the substrate-binding surface that we identified by sequence comparisons. Screening of this library using a newly developed MS-based high-throughput assay helped identify multiple enzyme variants that contained four substitutions and exhibited significant chitinolytic activity and a concomitant decrease in cellulolytic activity. The chitin-active variants became more rapidly inactivated during catalysis than a natural chitin-active AA10 LPMO, an observation likely indicative of suboptimal substrate binding leading to autocatalytic oxidative damage of these variants. These results reveal several structural determinants of LPMO substrate specificity and underpin the notion that productive substrate binding by these enzymes is complex, depending on a multitude of amino acids located on the substrate-binding surface.

Lytic polysaccharide monooxygenases (LPMOs) constitute a class of enzymes that employ a powerful oxidative mechanism to cleave glycosidic bonds within crystalline regions of recalcitrant biomasses, such as cellulose and chitin. After the discovery of their catalytic function in 2010 (1), LPMOs have been classified as auxiliary activities (AA) in the carbohydrate active enzymes database (cazy.org; (2)) where they are categorized in families AA9-11 and AA13-16 on the basis of sequence similarity. LPMOs are abundant in Nature, where they are frequently produced by fungi and bacteria involved in the degradation of structural polysaccharides in plants, crustaceans, fungi, insects and molluscs. Thus, LPMOs hold an important role in the Earth's carbon cycle. Some studies suggest alternative functions, including a role as virulence factors in microbial pathogenicity, that are not associated with biomass turnover (3-5).

LPMOs engage in a synergistic interplay with hydrolytic enzymes (e.g. cellulases and chitinases) during the conversion of recalcitrant polysaccharides, an important aspect of LPMO functionality that was observed prior to unravelling their mode of action (6,7). The crystalline surface of densely packed polysaccharides can be disrupted by the oxidative

action of LPMOs, thereby generating access points for hydrolytic enzymes in areas that otherwise would be less accessible (1,8-10). The resulting boosting effect on biomass turnover makes LPMOs key components in the development of industrial bioprocessing technology (11,12).

While some LPMOs are expressed as single catalytic domains, others are associated with a carbohydrate-binding module (CBM) through a flexible linker region (13). CBMs are thought to increase the effective enzyme concentration on the substrate surface by anchoring the catalytic domain in proximity of substrate binding sites (14,15). Two conserved histidines, one of which is the N-terminal amino acid of the mature LPMO, are located on the flat substrate-binding surface of the catalytic domain and constitute the catalytic centre of the LPMO. Together with the alpha amino group and a conserved tyrosine or phenylalanine in the axial position, these equatorial histidines coordinate a single copper ion, the reduction of which from Cu(II) to Cu(I) is crucial for catalysis (16). In fungal LPMOs the N-terminal histidine tends to be methylated (16) but this post-translational modification has not been observed in LPMOs of bacterial origin.

LPMO catalysis has generally been believed to require molecular oxygen and a reductant that delivers two electrons for each catalytic cycle (1,17,18). However, a recent study has indicated that LPMOs may employ H_2O_2 as co-substrate in a reaction that does not require two reductant-delivered electrons per cycle (19). While reduced LPMOs are prone to oxidative damage when exposed to high levels of O_2 or H_2O_2 in the absence of a proper substrate (19-21), well controlled H_2O_2-mediated reactions result in drastically improved catalytic rates (22) and stable reaction kinetics (12,23). Notably, under the conditions normally used in LPMO reactions, H_2O_2 will be formed either by O_2 reacting with reduced LPMO molecules that are not bound to the substrate (24,25) or by reactions involving O_2 and the reductant in the presence of trace amounts of transition metals.

LPMOs may be active on cellulose, hemicellulose, chitin, starch and/or oligosaccharides (26). Most known LPMOs are active on cellulose or chitin, which are among the most abundant polysaccharides on Earth, both consisting of β-1,4-linked monomers (glucose in cellulose and *N*-acetylglucosamine (GlcNAc) in chitin) rotated 180° relative to each other. LPMO-mediated cleavage of cellulose and chitin occurs by hydroxylation of the C1 or C4 carbon of the sugar monomers adjacent to the scissile glycosidic bond (1,16,27), and different LPMOs can be limited to one of these mechanisms or be capable of both. Oxidation of the C1 carbon results in the formation of 1,5-δ-lactones that are spontaneously converted to their more stable aldonic acid forms, while oxidation of the C4 carbon produces 4-ketoaldoses that are hydrated to their corresponding gemdiol form (25). Of note, for chitin, only C1 oxidation has been observed.

NMR-based studies of LPMO-substrate interactions (28,29), modelling (30), and mutational studies (20,30-33) suggest that precise arrangements of multiple amino acid side chains covering a major fraction of the substrate-binding surface dictate enzyme properties such as oxidative regioselectivity and substrate preferences. Simultaneously, these multi-side chain arrangements ensure stability for the LPMO by promoting precise substrate binding that protects the LPMO from oxidative self-inactivation (20). To create more insight into the structural determinants of LPMO substrate specificity, we have generated and screened a rationally designed mutant library to convert the cellulose-active LPMO10C from *Streptomyces coelicolor* A3(2) (hereinafter called *Sc*LPMO10C, previously known as CelS2 (34)) to a chitin-specific enzyme. The mutant library, containing multiple mutations at five positions on the substrate-binding surface (Fig. 1), was designed based on conservation patterns detected in 130 AA10 sequences (Table S1), including LPMOs acting on cellulose (C1-specific and mixed C1/C4-oxidizing), chitin (C1-specific), and LPMOs with as yet unknown substrate-specificity. The generated library, containing 4320 variants, was subsequently screened using a mass spectrometry based high-throughput assay for LPMO activity.

RESULTS

Library design and mutant generation

Library design was based on multiple criteria, one of which was restricting library size. Thus, we focused on residues for which there was experimental data indicating a role in substrate binding. Furthermore, library design was limited to positions for which it was possible to compare multiple LPMOs structurally, i.e., positions in regions where sequence alignments were reliable and structures were similar. The selected positions all occur in the loop region that is referred to as the "L2 loop", which covers a relatively large area on the flat substrate-binding surface of *Sc*LPMO10C and which contains most of the sequence variation at the LPMO surface. Figure 1 shows the location of residues Tyr79, Asn80, Phe82, Tyr111, and Trp141 (position 1-5) that were targeted for mutation. In terms of subsites, the mutations affect subsites -4 to -2, which are known to play an important role in substrate-binding, both in cellulose- (35) and chitin-active (30) LPMOs. These residues were postulated to dictate substrate specificity based on conservation patterns identified when comparing the sequences of cellulose- and chitin-active AA10 LPMOs, as outlined in Figure 1C. Furthermore, a ^{2}H/^{1}H exchange experiment had previously shown that Tyr54, Glu55, Gln57 and Thr111 in *Sm*LPMO10A (position 1-3 and 5, see below) interact with crystalline chitin (29). The selected positions showed limited natural variation (Fig. 1), which allowed us to cover the naturally used sequence space in a library of acceptable size. Of course, residues in other locations, e.g. on the "other" side of the active site (+ subsites) could also play a role in determining substrate specificity, but it is much more difficult to structurally compare LPMOs in this region.

Tyr79 (position 1) is the only aromatic residue on the AA10 substrate-binding surface that stacks with the carbohydrate substrate (-4 subsite in *Sm*LPMO10A (30)). This position has been targeted in recent site-directed mutagenesis studies which revealed its importance for both substrate binding (20,30) and enzyme activity and stability (20,31). The most common natural residues at this position are Tyr and Trp, but non-aromatic residues also occur. Thus, the Tyr at this position was mutated to Trp/Thr/Asp/Glu and Ala. Alanine substitutions were included at all positions.

The second position, Asn80 in *Sc*LPMO10C, was selected on the basis of being highly conserved in C1 and mixed C1/C4 oxidizing cellulose-active LPMO10s, and its different and strictly conserved nature in chitin-active LPMO10s, where it is a Glu. Mutation of this residue in chitin-oxidizing *Sm*LPMO10A resulted in strongly reduced substrate binding and abolished enzyme activity (6,20). In the library, Asn80 in *Sc*LPMO10C was mutated to residues with similar side chain size and polarity (Gln/Asp/Glu), as well as to Ser and Ala, which are also, but rarely, found at this position.

The third position, Phe82 in *Sc*LPMO10C, was recently shown to be important for the regioselectivity of cellulose oxidation in an LPMO10 with mixed C1/C4 activity (31). LPMO10s with mixed C1/C4-cellulose oxidation activity tend to have an Asn at this position (see Figure 1C), whereas those that are strict C1-oxidizers tends to have Phe (cellulose-oxidizers) or Gln (chitin-oxidizers) at this position. Of note, C1/C4 oxidizers active on cellulose tend to show activity on chitin, such as *Ma*LPMO10B from *Micromonospora aurantiaca*. Mutation of Asn85 in *Ma*LPMO10B to Phe almost abolished the C4-activity, but also the chitin-oxidizing activity (31), indicating an important role in substrate interactions. Position 3 was mutated to Ala/Gln/Asn/His/Tyr based on the natural variation in all types of LPMO10s.

Position 4, Tyr111 in *Sc*LPMO10C, is located in a less conserved loop in *Sc*LPMO10C and other cellulose C1-oxidizing LPMO10s. This extra loop (*Sc*LPMO10C_P110_Y111_D112) always comes with the upstream motif Asn-Trp-Phe (*Sc*LPMO10C-N80-W81-F82), which includes position 2 and 3. Position 4 was mutated to Ala/Phe/His to vary the side chain properties at this position.

The fifth position, Trp141 in *Sc*LPMO10C, is highly conserved within each of the LPMO10 substrate-specificity groups. While the typical chitin oxidizing LPMOs (e.g. *Sm*LPMO10A-like) tend to have a polar Thr at this position, the majority of LPMO10s with mixed activities (C1/C4 on cellulose and C1 on chitin) have a Gln and the strict C1-oxidizing cellulose-active LPMO10s (*Sc*LPMO10C-like) have a Trp at this position. Here, Trp141 was mutated to

Ala/Gln/Thr/Phe. The final library contained 4320 variants.

High-throughput library screening

Chitin-activity was measured using a high-throughput mass spectrometry-based assay for detection of oxidized chito-oligomers. An Agilent RapidFire 365 system was applied and the solid phase extraction and triple-quadropole mass spectrometry detection methods used were established based on reaction products generated by the positive control enzyme *Sm*LPMO10A (CBP21) acting on β-chitin as substrate. As there is no chromatographic separation between the analytes in the RapidFire system the triplequadrupole mass spectrometer was run in MRM mode in order to obtain maximum selectivity and sensitivity. Testing with a mixture of oxidized chito-oligosaccharides led to the identification of fragments that selectively represented the various oxidized species. The precursor ions used to fragment and subsequently quantify daughter fragments in the triplequadropol instrument were the $[M+H_2O-H^+]$-species of the aldonic acid forms of oxidized chitin oligomers consisting of 2 to 6 monomers (Figs. 2 and S2). Protocols for LPMO enzyme reactions in 384-well microplates were established using robotic liquid handling methods optimized to evenly distribute suspensions of solid β-chitin.

The designed LPMO library was expressed in *E. coli* XL10 Gold and screened for production of LPMOs with activity towards β-chitin as described in the Experimental procedures section. A primary screen of 11520 transformants led to selection of 42 transformants. After a second screening of these mutants for verification of activity and after discarding two mutants that contained unintended mutations discovered during sequencing, 37 transformants remained, representing 27 unique mutants, as detailed below.

Sequence analysis of putative chitin-active mutants

Table 1 provides sequence information for the 37 mutants that remained after the screening process. The collection contained 27 unique mutants, including two that were detected four times, one that was detected three times and two

that were detected twice. The combined frequencies of residues among all the 37 variants (Table 1A) and among the variants that were detected multiple times (Table 1B), suggested a consensus sequence for chitinolytic activity of Tyr, Asp, Xaa, Phe and Gln for positions 79, 80, 82, 111 and 141, respectively. At position 79, 95% of the selected variants had kept the wild-type amino acid. At the other four positions, mutation frequencies were higher and all were mutated, relative to wild-type *Sc*LPMO10C, in the deduced consensus sequence. Both N80 and Y111 were substituted in approximately 75% of the 37 mutants, with the most common substitutions being N80D and Y111F. Residue F82 was replaced by a variety of different amino acids in 95% of the putative chitin-active variants, and almost 50% of these carried the mutation F82Q. W141 was the only residue that was mutated in all selected variants, with W141Q being the most frequent substitution.

Based on these observations, a subset of the mutants that were detected multiple times and carried the mutation pattern Y79/D80/x82/F111/Q141 (M2, M5 and M18; Table 1C) were selected for production and further investigation. Of note, this mutation pattern was present in 11 of the 37 selected mutants. The contribution of individual mutations to chitinolytic activity was investigated by studying the effect of mutating single residues in M18, the most active variant (see below), back to the wild-type sequence. This required construction of two variants of M18, whereas the effect of the other reverse mutations could be assessed by characterization of variants that were among the 37 selected mutants (Table 1C).

Production of putative chitin-active mutants

The selected *Sc*LPMO10C variants and *Sc*LPMO10C wild-type were expressed and purified to electrophoretic homogeneity (Figure S3) using anion exchange purification followed by size exclusion chromatography. The yields of purified protein were typically 10-20 mg per litre culture.

Verification of chitinolytic activity

Analysis of reaction products after incubation of β-chitin with purified *Sc*LPMO10C variants containing the mutation pattern

4

Y79/D80/x82/F111/Q141 showed that the selected enzymes indeed were active towards chitin (Fig. 3). MALDI-ToF mass spectra of reaction products generated by the three mutants (Fig. 3D-F) were very similar to spectra of products generated by the well-known chitin-active LPMO from *Serratia marcescens* (*Sm*LPMO10A or CBP21) after degradation of β-chitin (Figure 3A,B). Comparison of the zoom-in views of the hexamer cluster (GlcNAc$_5$GlcNAc1A) for *Sm*LPMO10A (Figure 3B) and the three mutants (Figure 3D-F), show identical dominating signals representing the aldonic acid sodium adduct (*m/z* = 1276) and the disodium adduct of the aldonate (*m/z* = 1298). There are, however, some minor differences: next to the peak for the lactone form (*m/z* 1258), the spectra for the mutants show signals at *m/z* = 1256 and *m/z* = 1260 (see arrows in Figures 3D-F), which could indicate LPMO side activities, as discussed below. Using the same reaction set-up and analytical procedures, no oxidized chito-oligomers were detected for reactions with wild-type *Sc*LPMO10C (Figure 3C).

Quantitative analysis of chitin degradation

Monitoring of chitin degradation over time showed that the mutants generated oxidized products at an initial rate close to that of *Sm*LPMO10A and that the product yield obtained in reactions with the best mutant, M18, after four hours was about half of the yield obtained with *Sm*LPMO10A (Figure 4). Interestingly, a hardly detectable, but still significant amount of oxidized product was detected in the reaction with *Sc*LPMO10C wild-type, suggesting that the *Sc*LPMO10C wild-type has a hitherto undetected very weak intrinsic capability of cleaving chitin. Figure 4 shows that, while the mutants had good initial rates, product formation stopped earlier, compared to *Sm*LPMO10A. M18 was able to generate products over a longer period compared to M2 and M5.

The stagnation of the product formation could be caused by reductant-, substrate- or enzyme-related issues, and was investigated by adding fresh reductant, fresh substrate, or fresh enzyme to the reaction at a point where the product generation had stopped (Figure S4A). This experiment showed that enzyme inactivation is the primary reason for the cessation of product

formation, as only addition of fresh enzyme led to recovery of product generation (Figure S4B).

Thermostability of the mutants

The apparent melting temperatures (T_m) of the mutants were determined by monitoring the effect of temperature on the binding of a fluorescent dye (SYPRO orange), where increased binding of the dye (monitored in a real-time PCR machine) indicates exposure of the hydrophobic core of the protein upon unfolding. The melting curves in Figure 5 show that *Sm*LPMO10A (T_m = 71.2 °C) and *Sc*LPMO10C wild-type (64.1 °C) are more stable than M2 (52.5 °C), M5 (53.5 °C), and M18 (54.8 °C). The decreased thermal stability of the mutants is somewhat surprising as the mutants contain only four mutations relative to the wild-type that are all located on the protein surface. Still, the apparent melting temperatures of the mutants are well above the reaction temperature used in the experiments (i.e. 40 °C).

Oxidative stability in H$_2$O$_2$-driven reactions

Based on the recent finding that H_2O_2 is a relevant co-substrate of LPMOs (19), it is conceivable that LPMO products observed in reactions without added H_2O_2 are in fact generated through H_2O_2-mediated catalysis after H_2O_2 has been formed from O_2 (24,25). This would mean that the apparent initial reaction rates reflect the rate-limiting step of H_2O_2 generation from O_2.

H_2O_2 mediated catalysis was investigated in reactions with M18 by adding 15 μM H_2O_2 at 15 minute intervals (Fig. 6A). Reaction samples taken in between addition of fresh H_2O_2 (after 7.5, 22.5, 37.5 and 52.5 minutes) indicated that the reactions must be fast as both M18 and the positive control, *Sm*LPMO10A, had depleted the H_2O_2 in less than 7.5 minutes, meaning that the product yields did not increase any further until fresh H_2O_2 was added. Overall, the progress curves of Fig. 6A indicate that, initially, the *Sm*LPMO10A and M18 show similar catalytic rates, but that their stabilities differ, similar to what was concluded from Figure 4. Thus, *Sm*LPMO10A and M18 differ in terms of how much of the added H_2O_2 is consumed in productive LPMO reactions rather than in non-productive reactions with either ascorbic acid or

reduced LPMOs, where the latter may generate oxidative damage on the enzyme leading to enzyme inactivation (19, 20). This difference was even more prominent in reactions where the amount of added H_2O_2 was increased to 100 µM: in this case *Sm*LPMO10A still performed well, whereas M18 was almost immediately inactivated (Fig. S5; note that *Sm*LPMO10A generated much more products when fed with this higher amount of H_2O_2). Control reactions, displayed in Figure 6B showed that *Sm*LPMO10A, *Sc*LPMO10C wild-type and M18 were hardly active in reactions where H_2O_2 was replaced by water, emphasizing the importance of H_2O_2 to drive the reaction at these low initial ascorbic acid concentrations. In these control experiments, the two chitin-active LPMOs, *Sm*LPMO10A and M18, did show some product formation over time due to the repetitive addition of small amounts of ascorbic acid (Fig. 6D).

Fig. 6A shows that *Sm*LPMO10A stays active for the full hour of the reaction. In fact, product formation seems to increase over time, which may be due to the accumulation of ascorbic acid, leading to in situ H_2O_2 production and/or may reflect that soluble products are more easily released as the reaction progresses (37). To gain further insight in the utilization of H_2O_2 we determined the total amount of oxidized sites in the reaction mixtures. Figure 6C shows that *Sm*LPMO10A indeed generated slightly more than 60 µM oxidized products (of which 34.6% was soluble), in line with the total amount of added H_2O_2 being 60 µM. In contrast, M18 only generated approximately 35 µM product (of which 41.7% was soluble), indicating that almost half of the added H_2O_2 was not converted to products. Of note, a control experiment showed that product formation after one hour by M18 was similar in H_2O_2-driven reactions with 10 times less ascorbic acid (Fig. 6D), showing that both product formation and enzyme inactivation are driven by added H_2O_2 and that reduction of the LPMO is not rate-limiting.

It is conceivable that the higher frequency of enzyme-inactivation in M18 relative to *Sm*LPMO10A could be due to weaker substrate binding of the former, since non substrate-bound reduced LPMOs are susceptible to damaging reactions with H_2O_2. However, due to the presence of the CBM2, wild-type *Sc*LPMO10C binds well to chitin (Fig. S6; (38)), and so does M18 (which also has an intact CBM2). It would of course be interesting to assess binding of the catalytic domain of M18 to chitin and compare this with binding of the catalytic domain of the wild-type enzyme. However, despite many attempts, we have not been able to produce the catalytic domain of M18 alone (i.e., M18 without the linker and the CBM2).

Effect of individual mutations on chitinolytic activity

To investigate the contribution of each mutated residue to chitinolytic activity, M18 (Y79/D80/A82/F111/Q141) was used as template to reverse single mutations back to the wild-type sequence. Two of these combinations (M18_A82F and M18_F111Y) were already present amongst the mutants that had passed the screening process and could be produced directly from the library. The two other residue combinations (M18_D80N and M18_Q141W) were generated by site-directed mutagenesis. Progress curves (Figure 7) showed that none of these single mutations reduced the chitinolytic activity of M18 to the (very low) level of wild-type *Sc*LPMO10C, but all variants performed significantly worse than M18. This suggests a cumulative effect of the mutations. Similarly to the observations made when comparing M2 and M5 to M18 (Figure 4), the mutational effects seem to primarily relate to stability. Three of the mutants exhibited an initial rate very similar to M18, but became inactivated at earlier time points compared to M18, whereas M18_Q141W showed a slightly reduced initial rate and slightly retarded inactivation.

Residual cellulolytic activity

All variants generated C1-oxidized cello-oligomers upon degradation of phosphoric acid-swollen cellulose (PASC) (Figure 8). C4-oxidation did not occur, since there were no detectable levels of C4-oxidized products and since levels of native products, which may emerge from C4-oxidized products as a result of the high pH used during HPAEC (40), were low (Figure 8A). Even though cellulose-activity was not completely lost, the mutants exhibited a drastic decrease in cellulolytic activity compared to wild-type *Sc*LPMO10C (Figure 8B), with

product yields after four hours amounting to 3% to 7% of the yields obtained with the wild-type enzyme (set to 100% product yield). M18_Q141W stood out in that product yields were high (52.5% of wild-type levels) and because this variant showed stable kinetics, in contrast to all the other variants, which did not generate products after the first hour of incubation. Figure 8B shows that all mutants, except M18_Q141W were as good as inactive after 1 h of incubation, whereas wild-type *Sc*LPMO10C maintained activity also after 1 h. This indicates that the low activity on cellulose, resulting from the mutations needed to convert *Sc*LPMO10C into a chitin-active LPMO, is associated with reduced enzyme stability in reactions with cellulosic substrates.

When comparing the activity of M18 and *Sc*LPMO10C wild type on β-chitin and PASC, it is clear that the substrate specificity has been dramatically shifted towards a preference for chitin. While M18 only gave a relative yield of 6.2% compared to the wild-type enzyme (100%) on PASC, M18 produced a relative yield of 100% compared to the wild-type enzyme (1.4%) on β-chitin (Figure 9). This represents approximately a 16-fold decrease in cellulosic activity and approximately a 70-fold increase in chitinolytic activity (note that the estimated increase in chitinolytic activity is inaccurate as the product generation by the wild-type on chitin is close to the lower detection limit).

DISCUSSION

By screening of a rationally designed mutant library, we were able to convert *Sc*LPMO10C from an almost exclusively cellulose-active LPMO into a chitin-active LPMO with only weak remaining cellulose-activity. None of the chitin-active variants showed C4-oxidizing activity on cellulose, as is the case for naturally occurring AA10s that act on both cellulose and chitin. As such, M18 and some of the M18 derivatives are AA10 LPMOs that have never been encountered in Nature so far: exclusively C1-oxidizing and with activity on chitin and cellulose. In this respect, M18_Q141W stands out, since it retains much of the chitin-degrading ability of M18, while regaining much of the cellulose-degrading ability of *Sc*LPMO10C. Of note, while strictly

C1-oxidizing enzymes with activity on both chitin and cellulose have not been encountered among characterized naturally occurring AA10 LPMOs, a recently described LPMO of eukaryotic origin that is the founding member of the AA15 family (41) has these properties.

Despite the success of our approach, the selected mutants are not perfect chitin-active LPMOs in the sense that they become inactivated faster during catalysis, compared to e.g. natural chitin-active *Sm*LPMO10A. Recent mutagenesis studies on a chitin-active (20) and cellulose-active (13,31) AA10s have shown that a considerable fraction of mutations with a negative effect on LPMO performance primarily affect LPMO stability under turnover conditions. These studies showed clear correlations between decreased substrate-binding and increased inactivation. Bissaro et al. have shown that reduced LPMOs are prone to oxidative damage as a consequence of the formation of reactive oxygen species through reaction of the reduced copper with O_2 or H_2O_2 in the absence of substrate (19). Accordingly, in their mutational study, Loose at al. not only showed a correlation between decreased substrate binding and an increased rate of inactivation, but also that increased inactivation is correlated to increased auto-catalytic damage (i.e., chemical modification) of residues in the catalytic center (20).

Accumulating data indicate that the stability of LPMOs likely depends on the ability of the enzyme to precisely bind to the substrate in a way that confines the emerging highly powerful reactive oxygen species to only act productively, i.e. abstracting a hydrogen atom from the C1 in the scissile glycosidic bond. Modelling studies have shown that, indeed, binding of the correct substrate strongly confines the spatial orientation of the reactive oxygen species (30,42), whereas structural studies of the binding of oligomeric substrates to a fungal LPMO (43) have shown that binding of a preferred substrate leads to a more confined catalytic center compared to binding of a less preferred substrate. Thus, we propose, that binding of chitin to M18 is not yet "perfect". This will lead to imprecise coordination of reactive oxygen species in the space between the active site copper and the chemical bond that is to be cleaved, and may lead to oxidation of the active

site residues, which results in irreversible inactivation of the LPMO.

On the latter note, the MALDI-ToF analyses of Figure 3 show that the three tested mutants, and in particular the two less stable mutants, M2 and M5, generated minor amounts of unexpected products (at m/z 1256 and m/z 1260). Both these species, which could be a double oxidized and a native product, respectively, are almost or completely absent in the reaction with *Sm*LPMO10A. Although the origin and nature of these species remains unknown, it is conceivable that imprecise binding of the substrate, leading to less confinement of the reactive oxygen species, may lead to non-specific reactions giving unusual products. It is also possible that auto-catalytic damage to the catalytic center reduces enzyme specificity as the reaction progresses.

Accumulating data (20,31,32,44); this study) suggest that productive interactions between LPMOs and their polymeric substrates are governed by a multitude of interactions involving many of the residues in the substrate-binding surface. The four mutations in M18, relative to *Sc*LPMO10C wild-type, seem to have a cumulative effect on the chitinolytic activity as none of the single mutations back to wild-type abolished chitinolytic activity (Fig. 7). Additionally, all the tested *Sc*LPMO10C variants, except M18_Q141W, showed low relative cellulose-activities of 3-7% compared to the wild-type (Fig. 8). Residue 141 stood out in that it, alone, seemed to be a major determinant of cellulolytic activity, as shown by the high cellulose-activity of M18_Q141W. This is discussed further below.

Figure 10 provides structural models of LPMO variants interacting with chitin. While such models need to be used with care, they do shed some light on the mutational effects observed in this study. Tyr 111 (position 4) does not have an obvious analogue in the well-studied chitin-active *Sm*LPMO10A. Fig. 10C illustrates that the protruding hydroxyl group of the Tyr side chain may interfere with substrate binding and it is thus not surprising that this Tyr was mutated, mostly to Phe, in the large majority of selected chitin-active mutants. Of note, Figs. 10B-D show that, next to the S109-Y111 loop that includes Tyr111, *Sc*LPMO10C contains another surface loop, S182-R185, that may interfere with chitin

binding. It is possible that these two loops, which are absent or shorter in naturally occurring chitin-active AA10 LPMOs, need further modifications to improve the properties of the chitin-active M18 mutant.

The other four targeted residues all have similarly positioned analogues in natural chitin-active LPMOs. Both MD simulations (30) and NMR studies (29) have shown that residues Tyr54, Glu55, Gln57 and Thr111 in *Sm*LPMO10A (equivalent to Tyr79, Asn80, Phe82, and Trp141 in *Sc*LPMO10C) interact with chitin during catalysis (mainly in the -5 to -2 subsites; Fig. 10). Most LPMOs, including LPMOs belonging to other families (28,35) have an exposed aromatic residue near the -4 subsite that is important for substrate-binding. The seemingly general importance of this interaction is supported by the present study, since the corresponding residue in *Sc*LPMO10C, Tyr79 (position 1) was unchanged in 95% of the variants, while the other 5% carried a Trp. The preference for Tyr or Trp seems context dependent, since a previous study has shown that the Y79W mutation has hardly any effect on the cellulolytic activity of *Sc*LPMO10C, whereas mutating the Trp present at this position in the chitinolytic and cellulolytic C1/C4 oxidizing *Ma*LPMO10B to Tyr (Y82W) reduced activity on both chitin and cellulose (31).

Figure 10 does not reveal a possible explanation for the observation that the targeted asparagine residue (Asn80, position 2) of *Sc*LPMO10C was mutated to aspartate in 70% of the chitin-active mutants and in almost 90% of the mutants selected multiple times. Possibly, the resulting change in charge somehow affects the catalytic competence of the catalytic center, which, notably, is affected by substrate binding (35) and thus may vary for cellulose and chitin substrates. It is worth noting the Glu, which occurs at this position in *Sm*LPMO10A, was present in the library but was only found in one of the 37 selected variants.

The mutants did not show any clear consensus for position 3 (Phe82), but among the variants that were detected multiple times the most common mutation was F82Q (M2), followed by F82H (M5) and F82A (M18). It seems clear, that reduction of the size of the side chain at this position is beneficial for chitinolytic

8

activity, as the original Phe was replaced by a smaller residue in 95% of the selected mutants. Accordingly, a previous study had shown a negative effect of increasing the size of this residue in *Ma*LPMO10B (31). Phe82 is slightly buried in the surface and does not seem to interfere directly with substrate-binding (Fig. 10). However, the side chain of Phe82 is close to the side chain of Trp141 (closest distance 3.4 Å), and this latter residue is of major importance for substrate binding and specificity (Fig. 10).

Trp141 was the only residue that was mutated in all selected chitin-active variants, and nearly 50% of the mutants and 90% of the mutants occurring multiple times had the W141Q mutation in this position. While this substitution does not correspond well with threonine being present in the corresponding position of strictly chitin-active *Sm*LPMO10A-like LPMOs (Fig. 1C), it fits well with glutamine frequently being present in *Ma*LPMO10B-like LPMOs. Of note, Loose et al. (20) showed that mutating the corresponding residue in *Sm*LPMO10A (Thr111Ala) did not have a major impact on the activity, which could indicate that the primary reason for Trp not being favourable is its large size. Indeed, Fig. 10 shows that the large protruding side chain of Trp141 could interfere with chitin binding. The W141Q mutation alone drastically reduced the cellulolytic activity of *Sc*LPMO10C (31), but did not yield chitinolytic activity. Likewise, introduction of the Q141W mutation in M18 led to a minor reduction in chitinolytic activity, but a large increase in cellulolytic activity.

The discovery of the peroxygenase activity of LPMOs (19) has created discussions in the field as to the nature of the natural co-substrate of the LPMOs (45-47). It has been claimed that H_2O_2-driven reactions are less specific and lead to more enzyme damage than O_2-driven reactions (47), but this is disputed (21,46). While an in-depth discussion or experimental assessment of these issues is beyond the scope of the present study, it is important to note that Fig. 6 shows that both *Sm*LPMO10A and M18 exert peroxygenase activity. Importantly, also in this case, the primary difference between M18 and the natural chitin-active *Sm*LPMO10A lies in the lower stability of the former.

In conclusion, the results presented in this study reveal structural determinants of the substrate specificity of LPMOs. However, first and foremost, these results underpin the complexity of substrate specificity in these fascinating enzymes. Apparently, substrate specificity depends on a multitude of correctly positioned collaborating residues and, despite progress such as described here, rational design of substrate specificity seems not yet feasible. Intriguingly, the multitude of mutations needed to confer chitinolytic activity upon *Sc*LPMO10C and the rather poor properties of intermediate stages of evolution, raises questions as to how natural evolution of LPMOs takes place. Most importantly, the present results add to the notion that stability, provided by an optimized LPMO-substrate combination that protects the LPMO from entering off-pathway processes, really is a key determinant of LPMO performance.

EXPERIMENTAL PROCEDURES

Library design and generation of ScLPMO10C mutants

Based on conservation patterns detected in 130 AA10 sequences (Supporting Table S1), residues Tyr79, Asn80, Phe82, Tyr111 and Trp141 in the N-terminal AA10 domain of *Sc*LPMO10C (Uniprot ID; Q9RJY2) were selected as targets in the design of the library (see results section and Figure 1). In order to limit the library size, amino acid substitutions in these positions were restricted on the basis of naturally observed sequence variation. Mutations to alanine were also included. The substitutions were Ala/Trp/Thr/Asp/Glu for Tyr79, Ala/Asp/Glu/Gln/Ser for Asn80, Ala/Gln/Asn/His/Tyr for Phe82, Ala/Phe/His for Tyr111, and Ala/Thr/Gln/Phe for Trp141 (see Figure 1C). This implies a library size of 4320 variants. The library was synthesized by GeneArt® Combinatorial Libraries (Life Technologies), and the amplified library was cloned into plasmid pWW0 for controlled expression with the XylS/Pm system (48,49). The plasmids harbouring the *Sc*LPMO10C encoding mutant genes were subsequently transformed into the *E. coli* XL10 gold expression host.

9

High-throughput screening of the mutant library

Cultivation of the mutant library

The library, in *E. coli* XL10 gold, was spread on LA agar supplemented with 100 µg/mL Ampicillin to ensure single colonies. The agar plates were incubated at 37 °C overnight. Colonies were picked and inoculated to clear, flat, sterile polystyrene 384 microwell plates (Nunc 242757) containing 30 µL LB medium supplemented with 100 µg/mL Ampicillin using a Genetix QPixII robot. 11 520 colonies were picked and stored as glycerol stocks at -80 °C.

The 11 520 transformants were inoculated from the glycerol stocks using a Tecan Freedom EVO-2 200 robot system equipped with an MCA384 well pipetting tool, and cultivated in 96-well flat, polystyrene microwell plates (Greiner 655163) with Costar lids (Corning 3931). Each well contained 80 µL of a defined basic medium (Red Hi+YE basic medium; see Supporting Information) with 100 µg/mL Ampicillin and 2 µL inoculum. The microwell plates with cultures were incubated at 37 °C, at 90% relative humidity, 900 rpm, and 3 mm amplitude in an Infors HT Multitron Pro shaker incubator for 20 hours. To minimise evaporation, the microwell plates were incubated in stacks of 5 and wrapped in autoclave paper.

After incubation, 40 µL of defined induction medium (Red Hi+YE induction medium; see Supporting Information) supplemented with 1.5 mM m-toluate and 100 µg/mL ampicillin was added to the cultures using a Beckman Coulter Biomek NXP and SCARA robotic system. The cultures were then incubated at 16 °C, 900 rpm, for 24 hours, wrapped in autoclave paper. Upon this incubation, the cells were pelleted by centrifugation of the microwell plates at 4700 rpm ($3828 \times g$) for 20 minutes in a Thermo Scientific SL 40R laboratory centrifuge and supernatants were discarded. Release of proteins from the periplasmic space was promoted by addition of 120 µL ion-free water and a subsequent vortex-treatment using a Quantifoil Instruments GmbH BioShake 3000 elm, at 1200 rpm for 60 seconds. The cells were stored at -20 °C prior to screening, which implies that they were subjected to one freeze-thaw cycle. In preceding method optimization, this procedure (treatment with ion-free water and one freeze-thaw cycle) had been found to liberate sufficient amounts of correctly processed LPMO molecules from the periplasmic space.

Primary screen for enzyme activity

96-well microwell plates containing water-treated cells were thawed in room temperature. Enzyme assays were performed in 384-well deep microwell plates (Corning™ 3965 Costar™ 384-Well Storage Block). The Tecan robot system equipped with an MCA384 well pipetting tool was used to add 20 µL of substrate solution (4 mg/mL β-chitin in 100 mM ammonium acetate buffer supplemented with 2 mM ascorbic acid and 15.8 µM CuCl$_2$, pH 6.0) to each well of the 384-well plates. The Beckman and SCARA robot system was then used to add 20 µL thawed cell suspension to each well containing substrate solution (one well per transformant). The microwell plates were then sealed and given a short spin in the centrifuge to collect all sample and substrate solution in the bottom of the wells. Next, the plates were vortexed on a BioShake at 2000 rpm for 20 seconds to ensure proper mixing. The plates were then incubated over night at 40 °C, 1000 rpm, 3 mm amplitude in an Infors HT Multitron Pro shaker incubator. The enzyme reaction was stopped by addition of 160 µL 100% acetonitrile. Plates were re-sealed, vortexed at 2000 rpm for 20 seconds and centrifuged at 4700 rpm ($3828 \times g$) for 15 minutes to pellet insoluble material. 80 µL of precipitate-free supernatant was transferred to new 384 deep microwell plates and stored at -20 °C awaiting analysis.

The presence of soluble oxidized chitin-oligomers was assessed using an Agilent RapidFire 365 instrument (Agilent G9530A) coupled to an Agilent triple quadrupole mass spectrometry detector (Agilent G6490A). An Agilent Hilic Rapidfire cartridge (HILIC Type H1) was used as stationary phase in an SPE-fashion, whilst the mobile phases used to retain and elute the oxidized chitin oligomers were a 90-10 (v/v) mixture of acetonitrile-water and a 10-90 (v/v) mixture of acetonitrile-water, each with 0.1% (v/v) formic acid and applied using a flow rate of 1 mL/min, respectively. The mass spectrometer was equipped with an ESI ion source run in negative mode (Gas temperature: 220 °C, Gas flow: 20 L/min, Nebulizer:40 psi,

Sheath Gas Temperature: 400 °C, Sheath Gas Flow: 11 L/min, Capillary: 3300 V, Nozzle Voltage: 500 V, iFunnel High: 90; iFunnel Low 60V), and the chitin oligomers were quantified in MRM mode using the following mass transitions: DP2^{ox}, m/z 439.2 → m/z 116.0; DP3^{ox}, m/z 643.3 → m/z 625.3; DP4^{ox}, 845.3 m/z → m/z 668.2; DP5^{ox}, m/z 1048.2 → m/z 871.2; DP6^{ox}, m/z 1251.5 → m/z 871.3; where DPn^{ox}, stands for an oligomer of *N*-acetylglucosamine (GlcNAc) comprising n sugar residues of which one is oxidized to GlcNAc1A [e.g., DP3^{ox} stands for (GlcNAc)$_{n-1}$GlcNAc1A], and where the first m/z value given for each oligomer represents [M-H$^+$], where M is the mass of the aldonic acid.

Cultivation and screening of candidates selected for validation screening

42 out of the 11520 transformants were selected for further screening. The location of each selected candidate in the library was identified and selected clones were spread on petri dishes containing LA agar supplemented with 100 µg/mL Ampicillin to obtain single colonies. The agar plates were incubated at 37 °C overnight. Four single colonies were selected for each candidate and inoculated to 120 µL medium in 96-well flat, polystyrene microwell plates (Greiner 655163) with Costar lids (Corning 3931). Two parallels were made: one microwell plate with LB medium supplemented with 100 µg/mL Ampicillin for use as a glycerol stock and one microwell plate with defined medium (Red Hi+YE basic medium) supplied with 100 µg/mL Ampicillin for further screening. The validation screening was performed as described above and included eight wells with *E. coli* producing the wild type *Sc*LPMO10C-enzyme and four wells with *E. coli* without plasmid as controls. After the validation screening, three of the 42 initially selected transformants were discarded as they did not show chitinolytic activity.

Sequence analysis of selected variants

Single colonies of the 39 selected variants were inoculated in LB medium supplemented with 100 µg/mL Ampicillin and incubated at 37 °C and 200 rpm overnight. Glycerol stocks were prepared and stored at -80 °C, and plasmids were isolated using a NucleoSpin Plasmid kit (Macherey-Nagel, Düren, Germany) and sent for

Sanger sequencing (Eurofins GATC, Cologne, Germany). The sequence data was analysed in BioEdit (www.mbio.ncsu.edu/BioEdit/bioedit.html). Two variants contained unintended mutations, leaving 37 variants for further studies. After removing redundant sequences, 27 unique variants remained (see Results section for details).

Generation of additional ScLPMO10C mutants

The gene encoding the M18 mutant (Y79/D80/A82/F111/Q141) was transferred from the XylS/Pm controlled plasmid pWW0 to the pRSETB expression vector using the InFusion HD cloning kit (Clontech) as previously described for wild-type *Sc*LPMO10C (34). Transfer to this smaller plasmid was necessary to facilitate cloning of additional variants based on the M18 construct using the QuikChange II XL site-directed mutagenesis kit (Agilent Technologies). Then, two variants of M18 were produced to partially revert M18 to *Sc*LPMO10C-WT, M18_D80N and M18_Q141W. After verification of the sequences of the mutated plasmids by Sanger sequencing (see above) the plasmids were transformed into One Shot® BL21 Star™ (DE3) chemically competent *E. coli* cells (Invitrogen) for protein expression (see below).

Enzyme production

Expression with the XylS/Pm system (pWW0 vector)

A subset of the mutants were selected for production and were produced essentially as described in (49). Briefly, *E. coli* XL10 gold carrying a mutant plasmid was inoculated from a glycerol stock in 333 mL of a defined basic medium (Red Hi+YE basic medium) supplied with 100 µg/mL ampicillin and incubated at 37 °C and 200 rpm in a shake flask, overnight. After cooling the cultures on ice for five min, 167 mL of a defined induction medium (Red Hi+YE induction medium) with 100 µg/mL ampicillin and 1.5 mM m-toluate (the inducer molecule of the XylS/Pm expression system) were added and the incubation was continued at 16 °C and 200 rpm for another 24 hours. Cell pellets were harvested by centrifugation at 5000 × g for 15

11

minutes at 4 °C (Beckman Coulter Brea, California, USA), after which a periplasmic extract was prepared using an osmotic shock method (50). All LPMOs were expressed with a signal peptide that directs the proteins to the periplasmic space (34). During secretion the signal peptide is cleaved off, which results in mature enzymes that possess an N-terminal histidine that can coordinate the catalytic copper.

Expression with the pRSETB vector

For production of mutants M18_D80N and M18_Q141W generated in the pRSETB vector, cells from a glycerol stock were used to inoculate 500 mL Terrific Broth (TB) supplemented with 100 µg/mL ampicillin, followed by incubation at 37 °C for approximately 20 hours in a Harbinger system (Harbinger Biotechnology & Engineering, Markham, Canada). Note that expression was driven by leakiness of the T7 promoter and that no inducer molecule was added. Cells were harvested and a periplasmic extract was prepared as described above.

Protein purification

Periplasmic extracts containing the mature (i.e. signal peptide-free) proteins were filtered using 0.45 µm syringe filters (Sarstedt, Nümbrecht, Germany) and adjusted to 50 mM Tris-HCl (pH 7.5) after which the proteins were purified by anion exchange chromatography using an ÄKTA pure chromatography system (GE HealthCare, Chicago, USA) equipped with a 5-mL HiTrap DEAE FF column (GE Healthcare), with 50 mM Tris-HCl (pH 7.5) as running buffer. The proteins were eluted by applying a linear salt gradient (0-500 mM NaCl) over 60 column volumes (CV). Protein fractions were examined by SDS-PAGE (Bio-Rad, Hercules, California, USA) and relevant fractions were pooled and concentrated to 1 mL using 10,000 MWCO (Molecular Weight Cut-Off) Vivaspin ultrafiltration tubes (Sartorius, Göttingen, Germany). The proteins were further purified by size exclusion chromatography using a HiLoad 16/60 Superdex 75 column with a running buffer consisting of 50 mM Tris-HCl (pH 8.0) and 200 mM NaCl. Fractions containing the LPMO were concentrated using 10,000 MWCO Vivaspin ultrafiltration tubes (Sartorius) with simultaneous buffer exchange to 20 mM sodium phosphate buffer (pH 6.0). Protein purity was assessed by SDS-PAGE. Before being employed in enzymatic reactions, the purified LPMOs were saturated with Cu(II) by a 30 minute incubation with $CuSO_4$ in a 1:3 molar ratio (LPMO:Cu^{2+}), followed by desalting using PD Midi-Trap G-25 columns (GE Healthcare) equilibrated with 20 mM sodium phosphate (pH 6.0) to remove excess Cu^{2+}, as described previously (34). Protein concentrations were determined by measuring A_{280} (absorbance at 280 nm) in a spectrophotometer (Eppendorf Biophotometer, Eppendorf, Hamburg) and absorbances were converted to protein concentrations using theoretical extinction coefficients calculated with the ExPASy ProtParam tool. The purified and copper saturated LPMOs were stored at 4 °C.

Additional enzymes

The *Serratia marcescens* GH18 exo-chitinase *Sm*Chi18A and endo-chitinase *Sm*Chi18C, its GH20 chitobiase (*Sm*GH20) as well as its chitin-oxidizing AA10 LPMO (*Sm*LPMO10A, also known as CBP21) were expressed and purified as previously described (5,44,51). Full-length LPMO10C from *S. coelicolor* A3(2) (*Sc*LPMO10C) and a truncated variant lacking the CBM2 (*Sc*LPMO10C-CD) were produced and purified as previously described (34). Purified *Thermobifida fusca* GH5 endoglucanase *Tf*Cel5A (52) was provided as a kind gift from the late Prof. David Wilson (Cornell University, NY, USA).

Determination of apparent melting temperature (T_m)

The apparent melting temperature (T_m) of the proteins was determined according to a protein thermal shift assay (ThermoFisher Scientific) based on using the fluorescent dye SYPRO orange to monitor protein unfolding (39). The quantum yield of the dye is significantly increased upon binding to hydrophobic regions of the protein that become accessible as the protein unfolds. The fluorescence emission was monitored using a StepOnePlus real-time PCR machine (ThermoFisher Scientific). 0.1 g/L LPMO in 50 mM sodium phosphate buffer (pH 6.0) was heated in the presence of the dye in a 96-well plate from 25 °C to 99 °C over 50 minutes.

For each protein, the experiment was carried out in quadruplicates (i.e. n = 4).

Substrates

Activity was assessed on β-chitin and phosphoric acid swollen cellulose (PASC). β-chitin (extracted from squid pen and deproteinized, batch 20140101, France Chitin, Orange, France) was ball-milled and sieved in order to produce particles with a size < 0.85 mm. PASC was prepared from Avicel PH-101 (microcrystalline cellulose) as described by Wood (53).

Substrate binding assay

Protein binding to β-chitin was evaluated using a slightly modified variant of the A_{280} method described by (44). The binding mixtures contained 10 mg/mL β-chitin and 0.1 mg/mL protein in 50 mM sodium phosphate pH 6.0 and were incubated at 22 °C and 1000 rpm in an Eppendorf thermomixer (Eppendorf, Hamburg, Germany). Substrate binding was monitored by measuring the A_{280} of the supernatant at various time points, using aliquots that were taken from the binding reactions and immediately vacuum filtered over a 0.45 µm filter to separate unbound protein from protein bound to substrate. Theoretical extinction coefficients calculated with the ExPASy ProtParam tool were used to determine the protein concentration.

Chitin degradation experiments

Activity assays

Unless stated otherwise, reactions were performed in 50 mM sodium phosphate buffer (pH 6.0) in the presence of 1 mM ascorbic acid (reductant) at 40 °C and 800 rpm in an Eppendorf thermomixer. All reactions were performed in triplicates.

Qualitative analysis of chitinolytic activity

For the initial verification of chitinolytic activity, the mutants were incubated at 10 µM with 10 g/L β-chitin. Wild-type *Sc*LPMO10C and chitin-active *Sm*LPMO10A (CBP21) were included in the experiment as controls. After separation of the solid material by vacuum filtering through a 0.45 µm filter, supernatants

were analysed by MALDI-ToF (see below) for detection of oxidized chito-oligomers.

Quantitative analysis of β-chitin activity

For quantitative analysis of the activity towards β-chitin, the LPMOs were incubated at 1 µM with 10 g/L β-chitin for up to 24 hours. A purified endo-chitinase (ChiC from *S. marcescens*; *Sm*ChiC) was added to all reactions at 0.25 µM to facilitate solubilization of oxidized products, as low LPMO activity alone may not be sufficient to generate oxidized product that are sufficiently short to become soluble (13) Aliquots were withdrawn at selected time points and filtered before the soluble fraction was merged with an identical volume of a 1 µM solution of chitobiase from *S. marcescens* (*Sm*CHB) in 5 mM Tris-HCl (pH 8.0), followed by overnight incubation at 37 °C. The chitobiase, a GH20 β-hexosaminidase, cleaves off single GlcNAc units from chito-oligosaccharides until GlcNAc is the final product. If the chito-oligosaccharide is oxidized at the C1 position, the final product is an oxidized dimer (chitobionic acid) (5). As a result of this procedure, all soluble oxidized products are converted to chitobionic acid, which can easily be quantified. The products were analyzed using an UHPLC system (see below). In some cases, the total amount of oxidized sites was determined, as described in "*LPMO reactions with H_2O_2 feeding*".

Probing the cause of enzyme inactivation

Reactions were set up as above, and samples were collected and filtered after four hours and six hours. At six hours, the remaining reaction mixture was divided into three identical fractions, where fresh reductant (1 mM) was added to one fraction, fresh reductant and fresh substrate (10 g/L) to another, and fresh reductant and fresh LPMO (1 µM) to the third fraction. The incubation was continued overnight before stopping the reactions by filtration. All supernatants were subjected to a chitobiase treatment, as above, before product quantification using an UHPLC system (see below).

LPMO reactions with H_2O_2 feeding

The LPMOs were pre-incubated at 1 µM in 50 mM sodium phosphate (pH 6.0) containing 10 g/L β-chitin and at 1000 rpm for 10 minutes to

13

reach 40 °C. This pre-incubation was followed by addition of ascorbic acid to a final concentration of 100 µM to reduce the catalytic copper from the Cu(II) to the Cu(I) state. Addition of ascorbic acid was immediately followed by addition of H_2O_2 to a final concentration of 15 µM. Control reactions without added H_2O_2 were also included. Aliquots were withdrawn and immediately vacuum filtered every 7.5 minutes, and every 15 minutes a fresh batch of ascorbic acid and H_2O_2 was added subsequently to withdrawing an aliquot from the reaction. The H_2O_2-driven reactions were also carried out using different ascorbic acid concentrations (0-100 µM) and a higher H_2O_2 concentration (100 µM added every 20 minutes for 60 minutes). Reaction supernatants were subjected to chitobiase treatment, as above. At the final time point (60 minutes), next to preparing a product-containing supernatant by the usual filtration procedure, part of the (non-filtered) reaction mixture (containing both soluble and insoluble products) was boiled for 10 minutes at 98 °C to stop the LPMO reaction and merged with an identical volume of a chitinase cocktail (10 µM *Sm*ChiA, 6 µM *Sm*ChiC, 1 µM *Sm*CBH), followed by overnight incubation at 37 °C and 600 rpm. This treatment is sufficient to completely degrade all chitin and converts all oxidized products to chitobionic acid, as described above. The resulting hydrolysates were used to assess the total amount of oxidized products using UHPLC (see below).

Cellulose degradation experiments

The LPMOs were incubated at 1 µM with 5 g/L PASC, prepared from Avicel essentially as described in (53), and aliquots were taken and filtered after 1 and 4 hours. To facilitate quantification of the solubilized oxidized products, these products were treated with a cellulase that converts oxidized products of varying length to a mixture of shorter fragments, including oxidized dimers (GlcGlc1A) and trimers (Glc₂Glc1A). This conversion was achieved by an overnight incubation of solubilized cello-oligosaccharides with 0.5 µM of an endoglucanase (*Tf*Cel5A from *Thermobifida fusca*) at 37 °C. Subsequently, oxidized dimers (GlcGlc1A) and trimers (Glc₂Glc1A) were quantified by HPAEC-PAD (see below). An

aliquot not degraded with endoglucanase was also analysed.

Product analysis

MALDI-ToF analysis

Reaction supernatants were assayed qualitatively using a matrix-assisted laser desorption/ionization time-of-flight (MALDI-ToF) UltrafleXtreme mass spectrometer (Bruker Daltonics GmbH, Bremen, Germany) equipped with a Nitrogen 337-nm laser. Reaction products (1 µL) were applied to an MTP 384 ground steel target plate TF (Bruker Daltonics) and merged with 2 µL of 9 mg/mL of 2,5-dihydroxybenzoic acid (DHB) dissolved in 30% acetonitrile, followed by air-drying. Data collection and analysis were carried out using the Bruker FlexAnalysis software.

UHPLC analysis

Quantification of oxidized chitobiose was achieved using a Dionex Ultimate 3000 UHPLC system (DionexCorp., Sunnyvale, CA, USA) equipped with a Rezex RFQ-Fast Acid H⁺ (8%) 7.8×100 mm column (Phenomenex, Torrance, CA) operated at 85 °C. Sample components were eluted isocratically using 5 mM sulfuric acid as mobile phase, and were detected using UV absorption at 194 nm. Data collection and analysis were carried out with the Chromeleon 7.0 software. Standards were generated in-house by complete oxidation of N-acetyl-chitobiose (Megazyme; 95% purity) with a chitooligosaccharide oxidase from *Fusarium graminearum* (ChitO; (54)) as described previously (5).

HPAEC-PAD analysis

Oxidized products generated from cellulosic substrates were analysed by high-performance anion-exchange chromatography (HPAEC) using a Dionex™ ICS5000 system (Thermo Scientific, Sunnyvale, CA) equipped with a disposable electrochemical gold electrode and a CarboPac PA1 column (Dionex) operated with 0.1 M NaOH (eluent A) at a column temperature of 30 °C. A multistep linear gradient with increasing amounts of eluent B (0.1 M NaOH + 1 M NaOAc) was used to elute the products, going from 0–10% B over 10 min; 10–30% B over 25 min; 30–100%

B over 5 min; 100–0% B over 1 min; and 0% B (reconditioning) for 9 min. Data collection and analysis were carried out with the Chromeleon 7.0 software. For analysis of endoglucanase-treated samples containing only two oxidized products, oxidized cellobiose and cellotriose, a steeper gradient of eluent B was used, as follows: 0–10% B over 10 min; 10–14% B over 5 min; 14–30% B over 1 min; 30–100% B over 2 min; 100–0% B over 0.1 min; and 0% B (reconditioning) for 10.9 min. Cellobiose (Sigma Aldrich) and cellotriose (Megazyme) were used as substrates for production of the C1-oxidized standards cellobionic acid (GlcGlc1A) and cellotrionic acid (Glc$_2$Glc1A), respectively, by incubation with cellobiose dehydrogenase from *Myriococcum thermophilum* (*Mt*CDH) (55).

Author contribution
MSJ carried out and interpreted most of the experiments and wrote the manuscript; BB planned the work and designed the library; ZF planned the work, designed the library, carried out experiments and supervised the project; PC designed experiments and carried out experimental work; HS and GK supervised development of the methods for library screening, GKN participated in method development and carried out the library screening. HFK developed the high-throughput mass spectrometry method. GVK planned the project and interpreted results; VGHE planned and supervised the project, interpreted results and managed writing of the manuscript; all authors contributed to writing of the manuscript and have approved the final version for submission.

REFERENCES

1. Vaaje-Kolstad, G., Westereng, B., Horn, S. J., Liu, Z., Zhai, H., Sørlie, M., and Eijsink, V. G. H. (2010) An oxidative enzyme boosting the enzymatic conversion of recalcitrant polysaccharides. *Science* **330**, 219-222
2. Levasseur, A., Drula, E., Lombard, V., Coutinho, P. M., and Henrissat, B. (2013) Expansion of the enzymatic repertoire of the CAZy database to integrate auxiliary redox enzymes. *Biotechnol Biofuels* **6**, 41
3. Agostoni, M., Hangasky, J. A., and Marletta, M. A. (2017) Physiological and molecular understanding of bacterial polysaccharide monooxygenases. *Microbiol Mol Biol Rev* **81**
4. Paspaliari, D. K., Loose, J. S., Larsen, M. H., and Vaaje-Kolstad, G. (2015) *Listeria monocytogenes* has a functional chitinolytic system and an active lytic polysaccharide monooxygenase. *FEBS J* **282**, 921-936
5. Loose, J. S., Forsberg, Z., Fraaije, M. W., Eijsink, V. G., and Vaaje-Kolstad, G. (2014) A rapid quantitative activity assay shows that the *Vibrio cholerae* colonization factor GbpA is an active lytic polysaccharide monooxygenase. *FEBS Lett* **588**, 3435-3440
6. Vaaje-Kolstad, G., Horn, S. J., van Aalten, D. M., Synstad, B., and Eijsink, V. G. H. (2005) The non-catalytic chitin-binding protein CBP21 from *Serratia marcescens* is essential for chitin degradation. *J Biol Chem* **280**, 28492-28497
7. Harris, P. V., Welner, D., McFarland, K. C., Re, E., Navarro Poulsen, J. C., Brown, K., Salbo, R., Ding, H., Vlasenko, E., Merino, S., Xu, F., Cherry, J., Larsen, S., and Lo Leggio, L. (2010) Stimulation of lignocellulosic biomass hydrolysis by proteins of glycoside hydrolase family 61: structure and function of a large, enigmatic family. *Biochemistry* **49**, 3305-3316

8. Vermaas, J. V., Crowley, M. F., Beckham, G. T., and Payne, C. M. (2015) Effects of lytic polysaccharide monooxygenase oxidation on cellulose structure and binding of oxidized cellulose oligomers to cellulases. *J Phys Chem B* **119**, 6129-6143

9. Eibinger, M., Ganner, T., Bubner, P., Rosker, S., Kracher, D., Haltrich, D., Ludwig, R., Plank, H., and Nidetzky, B. (2014) Cellulose surface degradation by a lytic polysaccharide monooxygenase and its effect on cellulase hydrolytic efficiency. *J Biol Chem* **289**, 35929-35938

10. Eibinger, M., Sattelkow, J., Ganner, T., Plank, H., and Nidetzky, B. (2017) Single-molecule study of oxidative enzymatic deconstruction of cellulose. *Nat Commun* **8**, 894

11. Johansen, K. S. (2016) Discovery and industrial applications of lytic polysaccharide mono-oxygenases. *Biochem Soc Trans* **44**, 143-149

12. Müller, G., Chylenski, P., Bissaro, B., Eijsink, V. G. H., and Horn, S. J. (2018) The impact of hydrogen peroxide supply on LPMO activity and overall saccharification efficiency of a commercial cellulase cocktail. *Biotechnol Biofuels* **11**, 209

13. Courtade, G., Forsberg, Z., Heggset, E. B., Eijsink, V. G. H., and Aachmann, F. L. (2018) The carbohydrate-binding module and linker of a modular lytic polysaccharide monooxygenase promote localized cellulose oxidation. *J Biol Chem* **293**, 13006-13015

14. Boraston, A. B., Bolam, D. N., Gilbert, H. J., and Davies, G. J. (2004) Carbohydrate-binding modules: fine-tuning polysaccharide recognition. *Biochem J* **382**, 769-781

15. Herve, C., Rogowski, A., Blake, A. W., Marcus, S. E., Gilbert, H. J., and Knox, J. P. (2010) Carbohydrate-binding modules promote the enzymatic deconstruction of intact plant cell walls by targeting and proximity effects. *Proc Natl Acad Sci U S A* **107**, 15293-15298

16. Quinlan, R. J., Sweeney, M. D., Lo Leggio, L., Otten, H., Poulsen, J. C., Johansen, K. S., Krogh, K. B., Jorgensen, C. I., Tovborg, M., Anthonsen, A., Tryfona, T., Walter, C. P., Dupree, P., Xu, F., Davies, G. J., and Walton, P. H. (2011) Insights into the oxidative degradation of cellulose by a copper metalloenzyme that exploits biomass components. *Proc Natl Acad Sci U S A* **108**, 15079-15084

17. Kjaergaard, C. H., Qayyum, M. F., Wong, S. D., Xu, F., Hemsworth, G. R., Walton, D. J., Young, N. A., Davies, G. J., Walton, P. H., Johansen, K. S., Hodgson, K. O., Hedman, B., and Solomon, E. I. (2014) Spectroscopic and computational insight into the activation of O_2 by the mononuclear Cu center in polysaccharide monooxygenases. *Proc Natl Acad Sci U S A* **111**, 8797-8802

18. Beeson, W. T., Phillips, C. M., Cate, J. H., and Marletta, M. A. (2012) Oxidative cleavage of cellulose by fungal copper-dependent polysaccharide monooxygenases. *J Am Chem Soc* **134**, 890-892

19. Bissaro, B., Røhr, Å. K., Müller, G., Chylenski, P., Skaugen, M., Forsberg, Z., Horn, S. J., Vaaje-Kolstad, G., and Eijsink, V. G. H. (2017) Oxidative cleavage of polysaccharides by monocopper enzymes depends on H_2O_2. *Nat Chem Biol* **13**, 1123-1128

20. Loose, J. S. M., Arntzen, M. O., Bissaro, B., Ludwig, R., Eijsink, V. G. H., and Vaaje-Kolstad, G. (2018) Multipoint precision binding of substrate protects lytic polysaccharide monooxygenases from self-destructive off-pathway processes. *Biochemistry* **57**, 4114-4124

21. Eijsink, V. G. H., Petrović, D., Forsberg, Z., Mekasha, S., Røhr, Å. K., Várnai, A., Bissaro, B., and Vaaje-Kolstad, G. (2019) On the functional characterization of lytic polysaccharide monooxygenases (LPMOs). *Biotechnol Biofuels* **12**, 58

22. Kuusk, S., Bissaro, B., Kuusk, P., Forsberg, Z., Eijsink, V. G. H., Sørlie, M., and Väljamäe, P. (2018) Kinetics of H_2O_2-driven degradation of chitin by a bacterial lytic polysaccharide monooxygenase. *J Biol Chem* **293**, 12284

23. Hegnar, O. A., Petrović, D. M., Bissaro, B., Alfredsen, G., Várnai, A., and Eijsink, V. G. H. (2019) pH-dependent relationship between catalytic activity and hydrogen peroxide production shown via characterization of a lytic polysaccharide monooxygenase from *Gloeophyllum trabeum*. *Appl Environ Microbiol* **85**

24. Kittl, R., Kracher, D., Burgstaller, D., Haltrich, D., and Ludwig, R. (2012) Production of four *Neurospora crassa* lytic polysaccharide monooxygenases in *Pichia pastoris* monitored by a fluorimetric assay. *Biotechnol Biofuels* **5**, 79

25. Isaksen, T., Westereng, B., Aachmann, F. L., Agger, J. W., Kracher, D., Kittl, R., Ludwig, R., Haltrich, D., Eijsink, V. G. H., and Horn, S. J. (2014) A C4-oxidizing lytic polysaccharide monooxygenase cleaving both cellulose and cello-oligosaccharides. *J Biol Chem* **289**, 2632-2642

26. Tandrup, T., Frandsen, K. E. H., Johansen, K. S., Berrin, J. G., and Lo Leggio, L. (2018) Recent insights into lytic polysaccharide monooxygenases (LPMOs). *Biochem Soc Trans* **46**, 1431-1447

27. Phillips, C. M., Beeson, W. T., Cate, J. H., and Marletta, M. A. (2011) Cellobiose dehydrogenase and a copper-dependent polysaccharide monooxygenase potentiate cellulose degradation by *Neurospora crassa*. *ACS Chem Biol* **6**, 1399-1406

28. Courtade, G., Wimmer, R., Røhr, Å. K., Preims, M., Felice, A. K., Dimarogona, M., Vaaje-Kolstad, G., Sørlie, M., Sandgren, M., Ludwig, R., Eijsink, V. G. H., and Aachmann, F. L. (2016) Interactions of a fungal lytic polysaccharide monooxygenase with beta-glucan substrates and cellobiose dehydrogenase. *Proc Natl Acad Sci U S A* **113**, 5922-5927

29. Aachmann, F. L., Sørlie, M., Skjak-Braek, G., Eijsink, V. G., and Vaaje-Kolstad, G. (2012) NMR structure of a lytic polysaccharide monooxygenase provides insight into copper binding, protein dynamics, and substrate interactions. *Proc Natl Acad Sci U S A* **109**, 18779-18784

30. Bissaro, B., Isaksen, I., Vaaje-Kolstad, G., Eijsink, V. G. H., and Røhr, Å. K. (2018) How a lytic polysaccharide monooxygenase binds crystalline chitin. *Biochemistry* **57**, 1893-1906

31. Forsberg, Z., Bissaro, B., Gullesen, J., Dalhus, B., Vaaje-Kolstad, G., and Eijsink, V. G. H. (2018) Structural determinants of bacterial lytic polysaccharide monooxygenase functionality. *J Biol Chem* **293**, 1397-1412

32. Danneels, B., Tanghe, M., and Desmet, T. (2019) Structural features on the substrate-binding surface of fungal lytic polysaccharide monooxygenases determine their oxidative regioselectivity. *Biotechnol J* **14**, e1800211

33. Span, E. A., Suess, D. L. M., Deller, M. C., Britt, R. D., and Marletta, M. A. (2017) The role of the secondary coordination sphere in a fungal polysaccharide monooxygenase. *ACS Chem Biol* **12**, 1095-1103

34. Forsberg, Z., Mackenzie, A. K., Sørlie, M., Røhr, Å. K., Helland, R., Arvai, A. S., Vaaje-Kolstad, G., and Eijsink, V. G. H. (2014) Structural and functional characterization of a conserved pair of bacterial cellulose-oxidizing lytic polysaccharide monooxygenases. *Proc Natl Acad Sci U S A* **111**, 8446-8451

35. Frandsen, K. E., Simmons, T. J., Dupree, P., Poulsen, J. C., Hemsworth, G. R., Ciano, L., Johnston, E. M., Tovborg, M., Johansen, K. S., von Freiesleben, P., Marmuse, L., Fort, S., Cottaz, S., Driguez, H., Henrissat, B., Lenfant, N., Tuna, F., Baldansuren, A., Davies, G. J., Lo Leggio, L., and Walton, P. H. (2016) The molecular basis of polysaccharide cleavage by lytic polysaccharide monooxygenases. *Nat Chem Biol* **12**, 298-303

36. Crooks, G. E., Hon, G., Chandonia, J. M., and Brenner, S. E. (2004) WebLogo: a sequence logo generator. *Genome Res* **14**, 1188-1190

37. Frommhagen, M., Westphal, A. H., Hilgers, R., Koetsier, M. J., Hinz, S. W. A., Visser, J., Gruppen, H., van Berkel, W. J. H., and Kabel, M. A. (2018) Quantification of the catalytic performance of C1-cellulose-specific lytic polysaccharide monooxygenases. *Appl Microbiol Biotechnol* **102**, 1281-1295

38. Forsberg, Z., Røhr, Å. K., Mekasha, S., Andersson, K. K., Eijsink, V. G. H., Vaaje-Kolstad, G., and Sørlie, M. (2014) Comparative study of two chitin-active and two cellulose-active AA10-type lytic polysaccharide monooxygenases. *Biochemistry* **53**, 1647-1656

39. Huynh, K., and Partch, C. L. (2015) Analysis of protein stability and ligand interactions by thermal shift assay. *Curr Protoc Protein Sci* **79**, 28 29 21-14

40. Westereng, B., Arntzen, M. Ø., Aachmann, F. L., Várnai, A., Eijsink, V. G. H., and Agger, J. W. (2016) Simultaneous analysis of C1 and C4 oxidized oligosaccharides, the products of lytic polysaccharide monooxygenases acting on cellulose. *J Chromatogr A* **1445**, 46-54

41. Sabbadin, F., Hemsworth, G. R., Ciano, L., Henrissat, B., Dupree, P., Tryfona, T., Marques, R. D. S., Sweeney, S. T., Besser, K., Elias, L., Pesante, G., Li, Y., Dowle, A. A., Bates, R., Gomez, L. D., Simister, R., Davies, G. J., Walton, P. H., Bruce, N. C., and McQueen-Mason, S. J. (2018) An ancient family of lytic polysaccharide monooxygenases with roles in arthropod development and biomass digestion. *Nat Commun* **9**, 756

42. Wang, B., Johnston, E. M., Li, P., Shaik, S., Davies, G. J., Walton, P. H., and Rovira, C. (2018) QM/MM Studies into the H_2O_2-dependent activity of lytic polysaccharide monooxygenases: Evidence for the formation of a caged hydroxyl radical intermediate. *ACS Catalysis* **8**, 1346-1351

43. Simmons, T. J., Frandsen, K. E. H., Ciano, L., Tryfona, T., Lenfant, N., Poulsen, J. C., Wilson, L. F. L., Tandrup, T., Tovborg, M., Schnorr, K., Johansen, K. S., Henrissat, B., Walton, P. H., Lo Leggio, L., and Dupree, P. (2017) Structural and electronic determinants of lytic polysaccharide monooxygenase reactivity on polysaccharide substrates. *Nat Commun* **8**, 1064

44. Vaaje-Kolstad, G., Houston, D. R., Riemen, A. H., Eijsink, V. G. H., and van Aalten, D. M. (2005) Crystal structure and binding properties of the *Serratia marcescens* chitin-binding protein CBP21. *J Biol Chem* **280**, 11313-11319

45. Bissaro, B., Várnai, A., Røhr, Å. K., and Eijsink, V. G. H. (2018) Oxidoreductases and reactive oxygen species in conversion of lignocellulosic biomass. *Microbiol Mol Biol Rev* **82**

46. Forsberg, Z., Sørlie, M., Petrović, D., Courtade, G., Aachmann, F. L., Vaaje-Kolstad, G., Bissaro, B., Røhr, Å. K., and Eijsink, V. G. H. (2019) Polysaccharide degradation by lytic polysaccharide monooxygenases. *Curr Opin Struct Biol* **59**, 54-64

47. Hangasky, J. A., Iavarone, A. T., and Marletta, M. A. (2018) Reactivity of O_2 versus H_2O_2 with polysaccharide monooxygenases. *Proc Natl Acad Sci U S A* **115**, 4915-4920

48. Gawin, A., Valla, S., and Brautaset, T. (2017) The XylS/Pm regulator/promoter system and its use in fundamental studies of bacterial gene expression, recombinant protein production and metabolic engineering. *Microb Biotechnol* **10**, 702-718

49. Courtade, G., Le, S. B., Saetrom, G. I., Brautaset, T., and Aachmann, F. L. (2017) A novel expression system for lytic polysaccharide monooxygenases. *Carbohydr Res* **448**, 212-219

50. Manoil, C., and Beckwith, J. (1986) A genetic approach to analyzing membrane protein topology. *Science* **233**, 1403-1408

51. Mekasha, S., Byman, I. R., Lynch, C., Toupalová, H., Anděra, L., Næs, T., Vaaje-Kolstad, G., and Eijsink, V. G. H. (2017) Development of enzyme cocktails for complete saccharification of chitin using mono-component enzymes from *Serratia marcescens*. *Process Biochemistry* **56**, 132-138

52. Irwin, D. C., Spezio, M., Walker, L. P., and Wilson, D. B. (1993) Activity studies of eight purified cellulases: Specificity, synergism, and binding domain effects. *Biotechnol Bioeng* **42**, 1002-1013

53. Wood, T. M. (1988) Preparation of crystalline, amorphous, and dyed cellulase substrates. in *Methods in Enzymology*, Academic Press. pp 19-25

54. Heuts, D. P., Winter, R. T., Damsma, G. E., Janssen, D. B., and Fraaije, M. W. (2008) The role of double covalent flavin binding in chito-oligosaccharide oxidase from *Fusarium graminearum*. *Biochem J* **413**, 175-183

55. Zamocky, M., Schumann, C., Sygmund, C., O'Callaghan, J., Dobson, A. D., Ludwig, R., Haltrich, D., and Peterbauer, C. K. (2008) Cloning, sequence analysis and heterologous expression in *Pichia pastoris* of a gene encoding a thermostable cellobiose dehydrogenase from *Myriococcum thermophilum*. *Protein Expr Purif* **59**, 258-265

FOOTNOTES

The abbreviations used are: aldonic acid of cellobiose (GlcGlc1A); aldonic acid of chitobiose (GlcNAcGlcNAc1A); ascorbic acid (AscA); auxiliary activity (AA); carbohydrate binding-module (CBM); degree of polymerization (DP); glycoside hydrolase (GH); lytic polysaccharide monooxygenase (LPMO); phosphoric acid swollen cellulose (PASC); *Streptomyces coelicolor* (*Sc*); *Serratia marcescens* (*Sm*).

19

FIGURE LEGENDS

Figure 1. Structural overview of targeted residues in *Sc*LPMO10C. Panel A displays a side-view of the crystal structure of the catalytic domain of wild-type *Sc*LPMO10C (PDB ID: PDB 4OY7; (34)) with the substrate binding surface facing downwards. The side chains of residues targeted for mutation are shown with green-colored carbons whereas carbons in the side chains of the two histidines that coordinate the copper ion (orange sphere) are colored grey. Panel B shows the substrate-binding surface with residue numbering according to the PDB structure, which is used throughout this study. Note that His35 is the N-terminal residue of the mature protein and that the mutational work was carried out on the full-length enzyme that includes a family 2 CBM connected by a flexible Pro/Thr-rich linker (13). Panel C shows amino acid frequencies encountered at each mutated position (1-5) in multiple sequence alignments of sequences belonging to various LPMO10 subgroups: *Sc*LPMO10C-like (26 sequences; C1-oxidizing, cellulose), *Ma*LPMO10B-like (28 sequences; C1/C4 oxidation of cellulose and C1 oxidation of chitin) and *Sm*LPMO10A-like (49 sequences; C1-oxidizing, chitin). Position 4 (*Sc*LPMO10C_Y111) is exclusively found in some *Sc*LPMO10C-like sequences and is always present with the upstream motif Asn-Trp-Phe in which the first and the last make up positions 2 and 3 in the library. Mutations included in the library are shown in the top right corner of the Figure. Panels A and B were made using PyMOL and the graphs in panel C were generated using WebLogo (36). A blue star in panels A-C marks the location of the second histidine (His144) of the histidine brace. See Table S1 for the sequences used in the analyses and Figure S1 for a structural comparison of natural LPMO10s with experimentally verified different substrate specificities.

Figure 2. Screening for chitinolytic activity. Chitinolytic activity was assessed using 2 g/L β-chitin and 1 mM ascorbic acid (reductant) at pH 6.0 and 40 °C. The figure show RapidFire ESI triple quadrupole MRM chromatograms for M2 (four independent wells, light green) and wild-type *Sc*LPMO10C (four independent wells, grey). The ESI MRM intensity is given on the y-axis while time (seconds) is on the x-axis; note the different scales on the y-axis. Chromatograms A-E show: A) DP2^{ox}: ESI MRM m/z 439.2 → m/z 116.0, B) DP3^{ox}: m/z 643.3 → m/z 625.3, C) DP4^{ox}: 845.3 m/z → m/z 668.2, D) DP5^{ox}: m/z 1048.2 → m/z 871.2, E) DP6^{ox}: m/z 1251.5 → m/z 871.3. Underlying spectral data are shown in Fig. S2. A clone was defined as positive if, for at least one oxidized product, the difference between the average of the green peaks was higher than the average of the grey peaks by at least ten times the standard deviation in the average for the grey peaks. The picture shows that the developed method failed for DP3^{ox}, which shows similar signals for M2 and *Sc*LPMO10C.

Figure 3. Oxidized products generated from chitin. Panel A shows the results of MALDI-ToF MS analysis after a 24 hours incubation of the positive control LPMO (*Sm*LPMO10A) with 10 g/L β-chitin at 40 °C in sodium phosphate pH 6.0 in the presence of 1 mM ascorbic acid (reducing agent) and displays the C1-oxidized products (aldonic acids and lactones) that can be expected for a chitin-active LPMO. Peaks representing oxidized chitooligomers are marked with their *m/z* value (see panel A for details). Panel B shows a zoom-in view of the hexamer cluster displaying *Sm*LPMO10A-generated products within the 1250 to 1320 *m/z* range. The peaks that are marked with an asterisk represent potassium adducts, which are absent in the spectra for the *Sc*LPMO10C mutants due to different storage buffers (*Sm*LPMO10A was stored in potassium phosphate pH 6.0, and the *Sc*LPMO10C mutants in sodium phosphate pH 6.0). Panel C shows a zoom-in view of the hexamer cluster area for wild-type *Sc*LPMO10C and shows no oxidized products. Panels D-F display zoom-in views of the hexamer cluster area for mutants M2, M5, and M18, respectively. Arrows in panels D-F indicate minor signals at *m/z* = 1256 and *m/z* = 1260 that are more prominent in the mutants (relative to the signals for regular oxidized products) compared to *Sm*LPMO10A.

Figure 4. Time course of chitin degradation. *Sm*LPMO10A, *Sc*LPMO10C wild-type, and the three chitin-active *Sc*LPMO10C variants M2, M5 and M18 were incubated at 1 µM with 10 g/L β-chitin at 40 °C and pH 6.0 in the presence of 1 mM ascorbic acid (reducing agent) for 4 hours. A chitinase (*Sm*ChiC) was also

20

added at 0.25 µM to obtain more rapid solubilization of LPMO generated chain ends from the insoluble substrate. The reaction was stopped by vacuum filtering and the soluble oxidized products were converted to oxidized dimers by treatment with chitobiase prior to analysis. All reactions were performed in triplicates. The error bars show ± S.D. (n = 3).

Figure 5. Mutational effects on thermostability. The plots show the apparent melting temperature (T_m) of copper-saturated *Sm*LPMO10A, *Sc*LPMO10C wild-type, M2, M5 and M18. The derivative of the fluorescence signal (-dRFU/dT, where "RFU" stands for relative fluorescence units") is plotted as a function of the temperature (39). The reactions contained 0.1 g/L LPMO and were heated from 25 °C to 99 °C, at a rate of 1.5 °C /min, in the presence of a fluorescent dye (SYPRO orange). The scans were performed four times for each protein and the Figures show a typical scan. All apparent melting temperatures (T_m) had standard deviations below ±0.1 °C.

Figure 6. H_2O_2 as co-substrate. Panel A shows the amount of solubilized oxidized sites produced by *Sm*LPMO10A (black line), M18 (dashed black line) and *Sc*LPMO10C wild-type (dotted grey line) over 60 minutes in a reaction with 10 g/L β-chitin in 50 mM sodium phosphate pH 6.0, that were supplied with 100 µM ascorbic acid (AscA) and 15 µM H_2O_2 every 15 minutes (indicated by arrows). The enzyme concentration was 1 µM in all cases. Aliquots were withdrawn both in between H_2O_2 additions (at 7.5 min, 22.5 min, 37.5 min and 52.5 min) and immediately prior to addition of fresh H_2O_2 (at 0 min, 15 min, 30 min, and 45 min). The apparent plateaus in product levels between the intermediate sampling points (e.g. at 7.5 min) and the subsequent point of addition of fresh H_2O_2 and AscA (e.g. at 15 min) are due to the fact that all H_2O_2 added at the preceding addition (in this example, 0 min) was consumed at the intermediate sampling point (7.5 min). The lines connecting the points are drawn for illustration purposes only and actual reaction rates were higher than suggested by the slopes of the ascending lines. Panel B shows control reactions related to Panel A. In the reactions labelled "without H_2O_2", water was added to the reactions instead of H_2O_2. The graph also shows H_2O_2-driven product formation by wild-type *Sc*LPMO10C (same curve as in Fig. 6A). Note the difference in the scale of the Y-axis between panels A and B; the product levels shown in panel B are very low, making quantification difficult. Panel C shows the total amounts of oxidized sites at the end of the reactions shown in panel A (i.e. after 60 min). Panel D shows the effect of varying the amount of added ascorbic acid in the reactions displayed in panel A (addition of 15 µM H_2O_2 + varying amounts of AscA every 15 minutes) for M18, and shows that essentially similar product yields were obtained when using a 10 times lower AscA concentration compared to the reactions shown in panel A. The control reaction to the left show that the LPMO is essentially inactive in the absence of added reductant. All reactions were performed in triplicates, and the error bars show ± S.D. (n = 3). Prior to analysis soluble oxidized products were converted to oxidized dimers by treatment with a chitobiase. The total amount of oxidized products was determined by treating the complete reaction mixture with a cocktail of chitinases and chitobiase, which leads to complete solubilization of the chitin and to conversion of all oxidized products, soluble or insoluble (i.e., still part of the chitin), to chitobionic acid.

Figure 7. Effect of single mutations on chitin degradation by M18. *Sc*LPMO10C wild-type, M18 and the four M18 mutants were incubated at 1 µM with 10 g/L β-chitin at 40 °C in 50 mM sodium phosphate buffer (pH 6.0) in the presence of 1 mM ascorbic acid for 24 hours. *Sm*ChiC was also added, at 0.25 µM, to obtain more rapid solubilisation of LPMO-generated oxidized chain ends from the insoluble substrate. The reaction was stopped by filtration and soluble oxidized products were degraded to oxidized dimers with chitobiase prior to analysis. All reactions were performed in triplicates. The error bars show ± S.D. (n = 3).

Figure 8. Residual cellulolytic activity. *Sc*LPMO10C wild-type and mutants were incubated at 1 µM with 5 g/L PASC and 1 mM ascorbic acid at 40 °C and in 50 mM sodium phosphate (pH 6.0). Panel A shows oxidized products after approximately 24 hours of incubation, varying from the dimer (GlcGlc1A) to the octamer (Glc₇Glc1A) generated by *Sc*LPMO10C wild-type, M2, M5 and M18. The background signal of the substrate (PASC) incubated with LPMO in the absence of reductant is also shown. Note that the size of

21

the peaks of the wild-type chromatogram was reduced by 25% before making the plot. Regions where C4-oxidized products would elute are marked. Panel B shows the amount of soluble oxidized sites in aliquots that were withdrawn after 1 hour and 4 hours of incubation; in this case oxidized products were quantified after degrading them to a mixture of oxidized dimers (GlcGlc1A) and trimers (Glc$_2$Glc1A) only, by treatment with the endoglucanase *Tf*Cel5A. Relative activities were calculated relative to the amount of product generated by the wild-type enzyme after four hours (100%). Testing of the cellulolytic activity of M18 with Avicel gave similar results. All reactions were performed in triplicates, and the error bars show ± S.D. (n = 3).

Figure 9. Comparison of chitinolytic and cellulolytic activity. Comparison of solubilized oxidized products generated in 4 hours by 1 µM M18 or 1 µM *Sc*LPMO10C wild-type from PASC (5 g/L) or β-chitin (10 g/L). 100% activity for *Sc*LPMO10C wild-type on PASC is equal to 218.6 µM (sum of GlcGlc1A and Glc$_2$Glc1A, obtained after cellulase treatment of soluble products as described in Experimental procedures). 100% activity for M18 on β-chitin is equal to 20.6 µM (GlcNAcGlcNAc1A, obtained after chitobiase treatment of soluble products as described in Experimental procedures). The solubilized oxidized products were converted to oxidized dimers before quantification. Note that quantification of products generated from β-chitin by the wild-type enzyme is inaccurate as the product levels are close to the lower detection limit. All reactions were performed in triplicates, and the error bars show ± S.D. (n = 3).

Figure 10. Models of substrate binding by LPMOs. Panel A shows a model (extracted from MD simulations performed on β-chitin (30)) of *Sm*LPMO10A interacting with GlcNAc$_7$. The side chains of the copper binding histidines and four of the five residues that were targeted for mutagenesis in cellulose-active *Sc*LPMO10C are shown as sticks (the shown residues correspond to Tyr79, Asn80, Phe82 and Trp141 in *Sc*LPMO10C; Tyr111 in *Sc*LPMO10C does not have an analogue in *Sm*LPMO10A). Panel B shows a model of M18 interacting with GlcNAc$_7$ that was generated by superposing the crystal structure of the catalytic domain of *Sc*LPMO10C onto the existing *Sm*LPMO10A-chitin model. The mutations found in M18 were introduced using the mutagenesis tool in PyMol and rotamers with the highest probabilities were selected. Panel C shows the same model for wild-type *Sc*LPMO10C, showing that two aromatic residues (Tyr111 and Trp141), which are both mutated in M18, may restrict contact with the chitin substrate. Panels B-D highlight two loop regions, Ser109-Pro110-Tyr111 and Ser182-Pro183-Gly184-Thr185 (red in panel B-D) that are extended in *Sc*LPMO10C, relative to natural chitin-active LPMOs, and which may interfere with chitin binding. Panel D shows a superposition of wild-type *Sc*LPMO10C (green and red) and *Sm*LPMO10A (grey) bound to β-chitin (yellow). The structures shown in Panel D are rotated 90-degrees clockwise relative to the structures shown in panels A-C.

TABLES

Table 1. Sequence analysis and selection of mutants. Table 1A shows the frequency of different substitutions of the targeted residues (Tyr79, Asn80, Phe82, Tyr111, and Trp141) in the 37 selected putatively chitin-active mutants. Mutations included in the library are shown below the boxes. Note that for most variants chitin-activity was not verified experimentally beyond the screening procedure, so the presence of false positives cannot be excluded. Table 1B shows the frequency of different substitutions in variants that occurred multiple times. Table 1C shows the three mutants (M2, M5 and M18) that were selected for further analysis, as well as four additional mutants that were generated by site-directed mutagenesis or selected from the mutant collection to verify the contribution of individual residues to the chitin-activity of M18. Darker shading of certain residues indicates identity with the wild-type residue.

A

Residue

	1	2	3	4	5
	79	80	82	111	141
*Sc*LPMO10C wt	Y	N	F	Y	W
substitutions in chitin-active mutants	95% Y 5% W	70% D 27% N 3% E	49% Q 24% H 14% N 8% A 5% F	62% F 27% Y 5% A 5% H	51% Q 38% A 11% T
	A/W/T/D/E	A/D/E/Q/S	A/Q/N/H/Y	A/F/H	A/T/Q/F

B

	79	80	82	111	141
variants occurring multiple times	100% Y	87% D 13% N	60% Q 27% H 13% A	80% F 20% Y	87% Q 13% A
	A/W/T/D/E	A/D/E/Q/S	A/Q/N/H/Y	A/F/H	A/T/Q/F

C

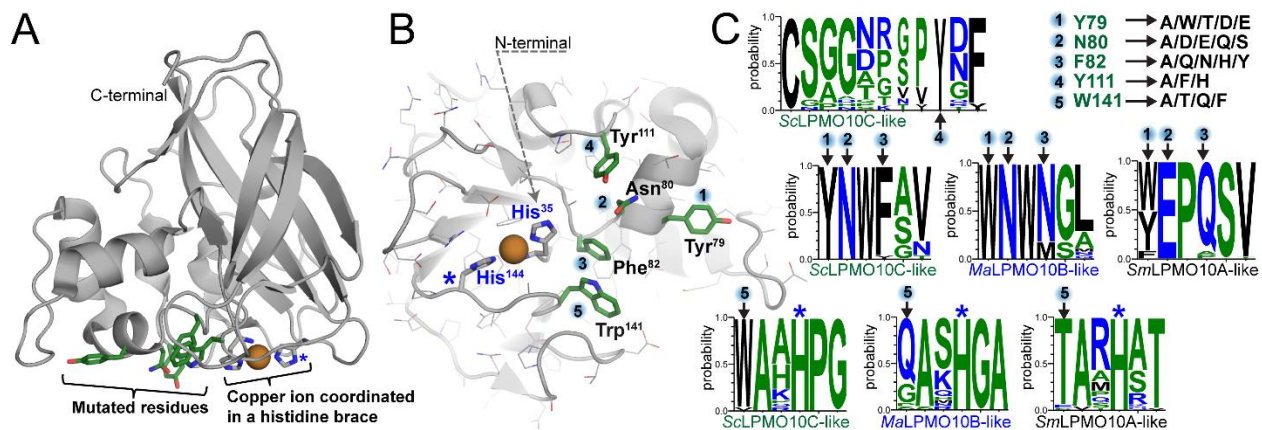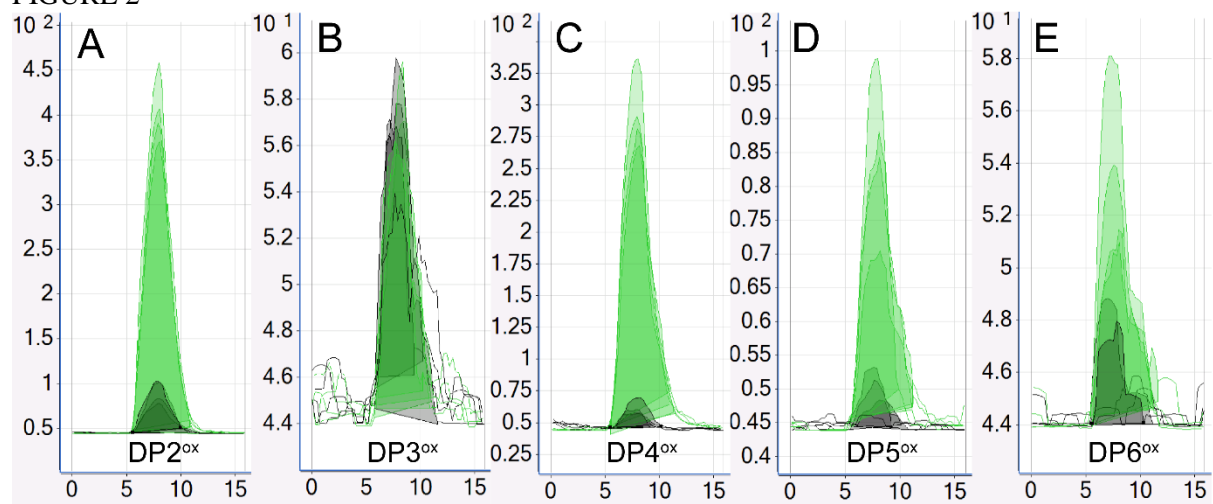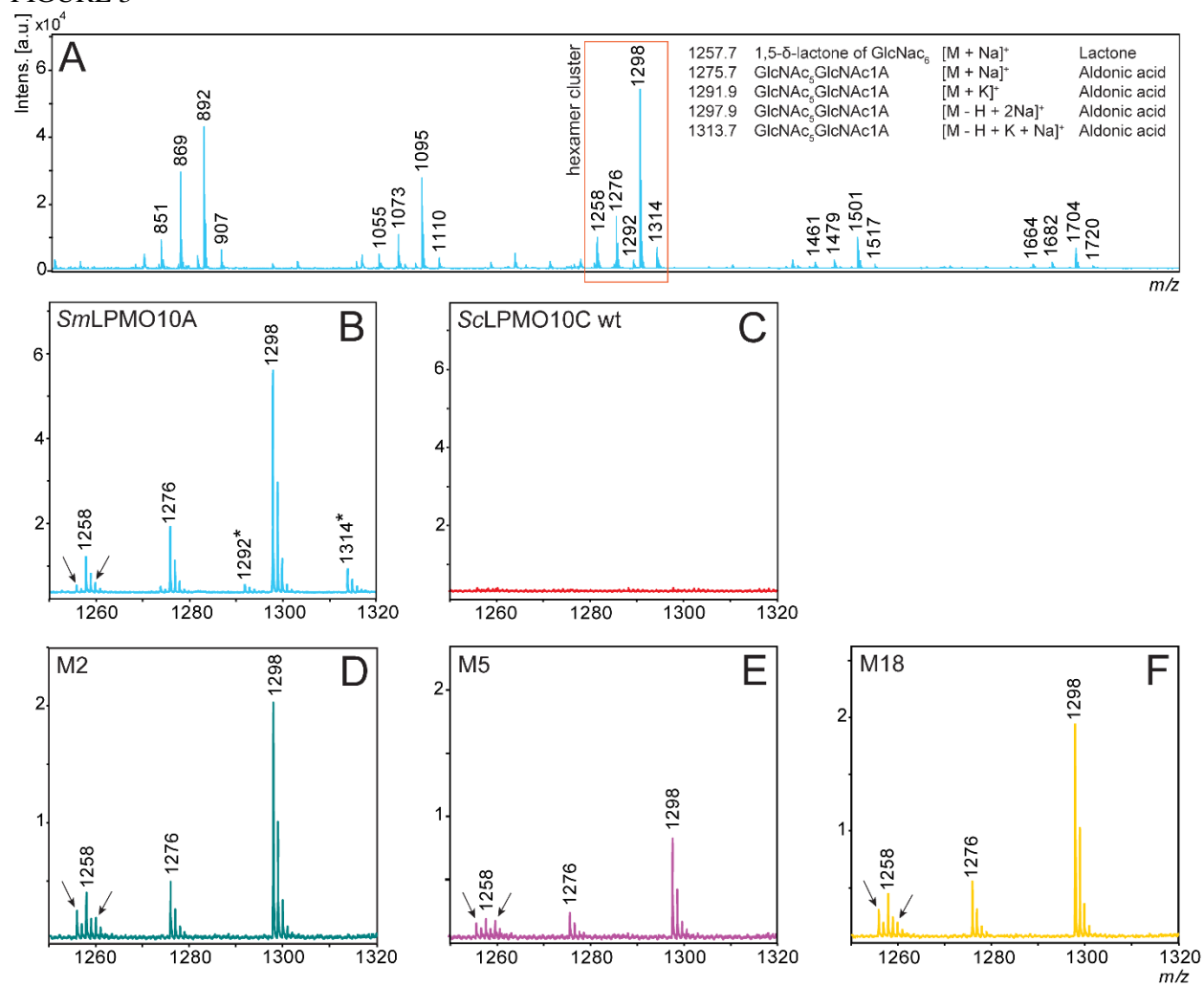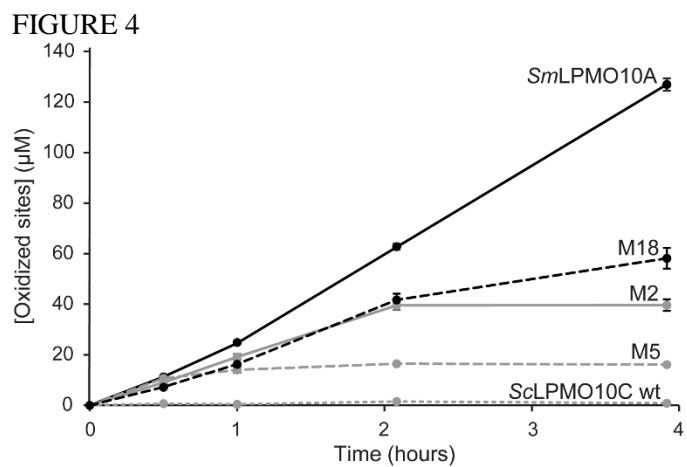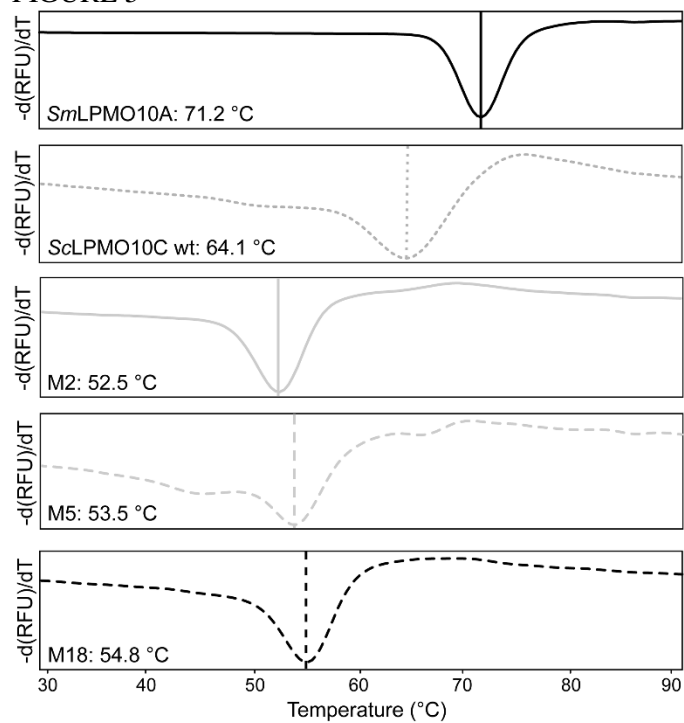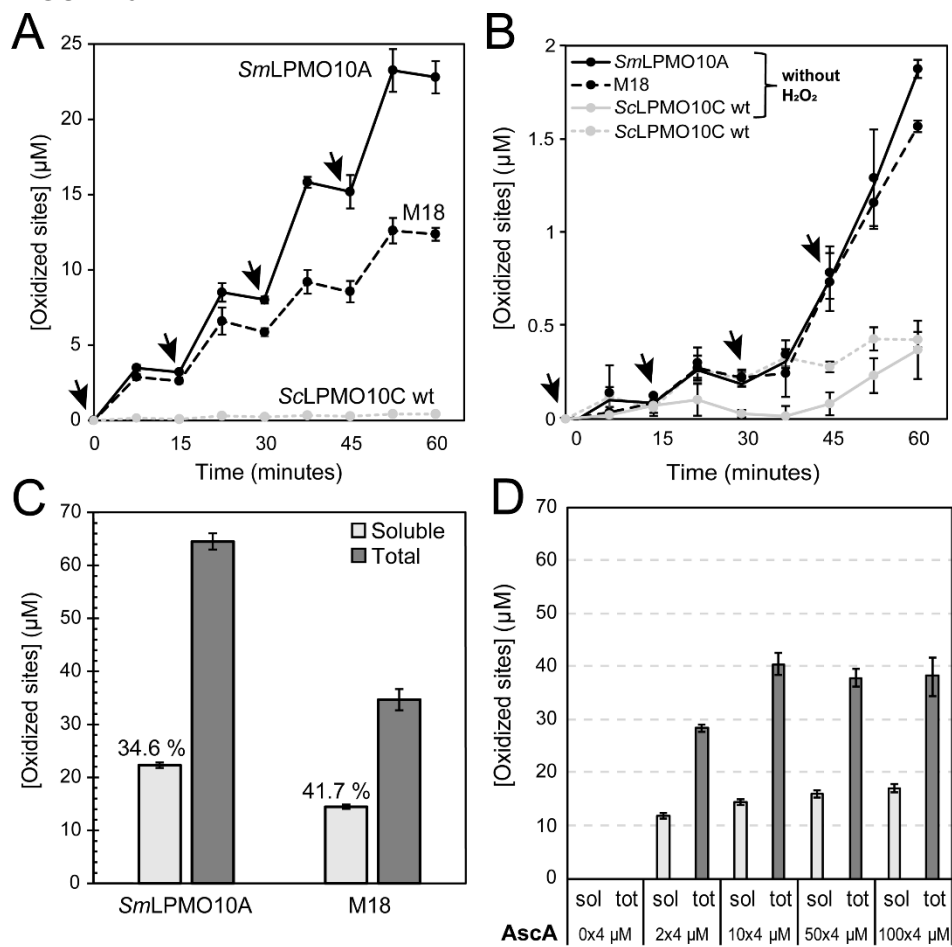|	79	80	82	111	141
M2	Y	D	Q	F	Q
M5	Y	D	H	F	Q
M18	Y	D	A	F	Q
M18_D80N	Y	N	A	F	Q
M18_A82F	Y	D	F	F	Q
M18_F111Y	Y	D	A	Y	Q
M18_Q141W	Y	D	A	F	W
*Sc*LPMO10C-wt	Y	N	F	Y	W

FIGURES

FIGURE 1

FIGURE 2

25

FIGURE 3

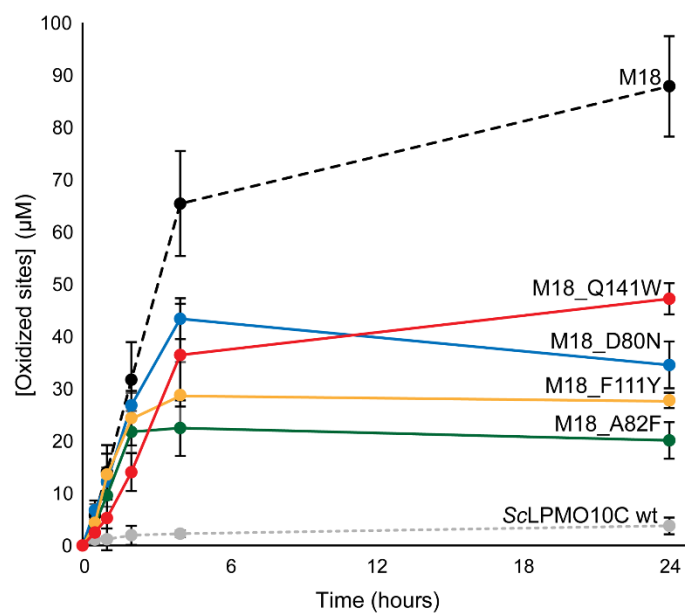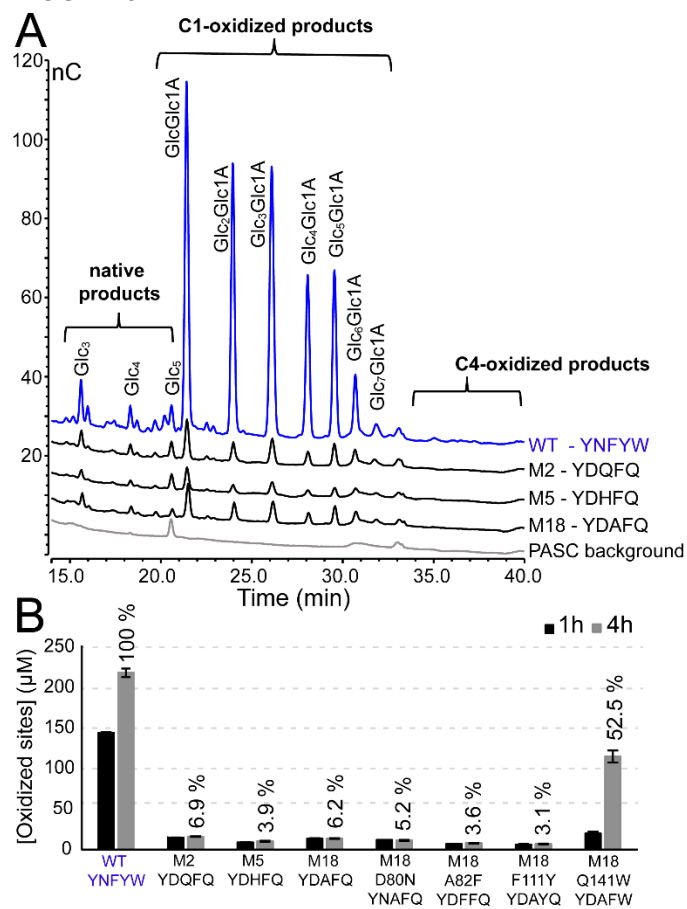FIGURE 4

FIGURE 5

FIGURE 6

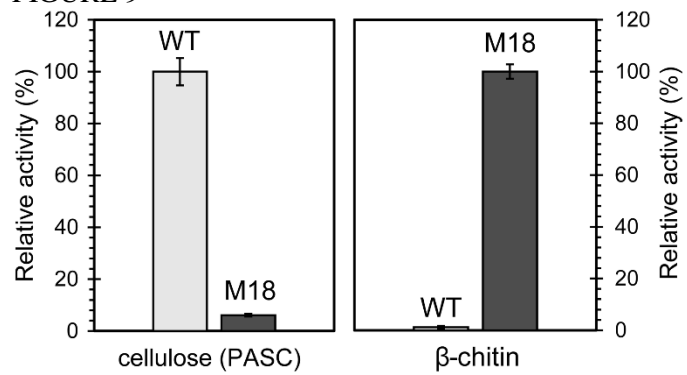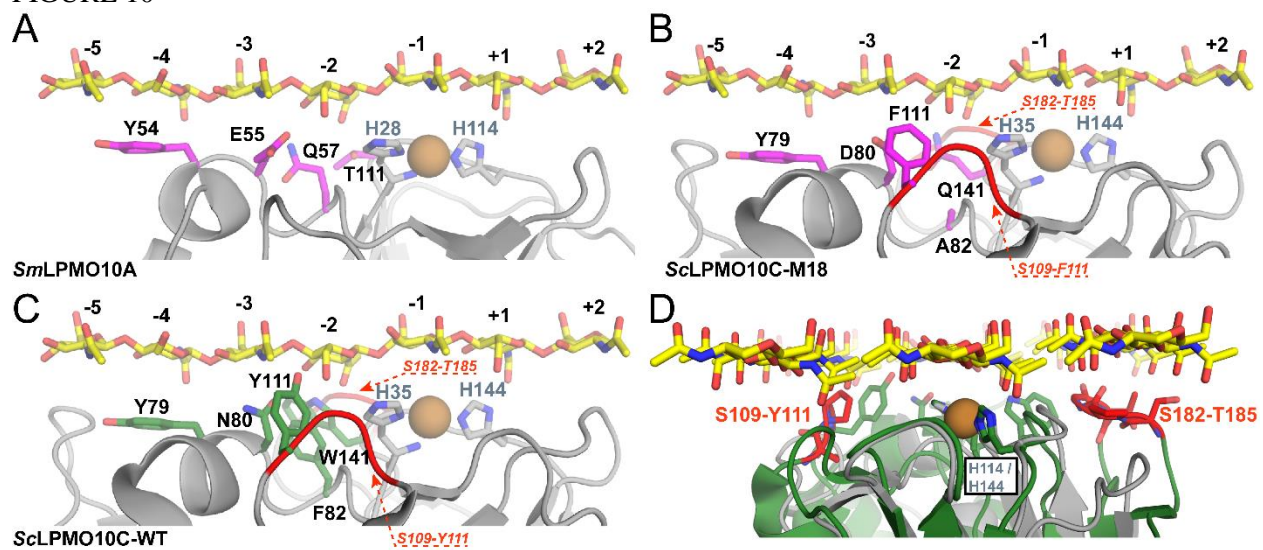FIGURE 7

FIGURE 8

FIGURE 9

32

FIGURE 10

Engineering chitinolytic activity into a cellulose-active lytic polysaccharide monooxygenase provides insights into substrate specificity

Marianne Slang Jensen, Geir Klinkenberg, Bastien Bissaro, Piotr Chylenski, Gustav Vaaje-Kolstad, Hans Fredrik Kvitvang, Guro Kruge Nærdal, Haavard Sletta, Zarah Forsberg and Vincent G. H. Eijsink

Alerts:
- When this article is cited
- When a correction for this article is posted

Click here to choose from all of JBC's e-mail alerts